Received: 29 December 2020 | Revised: 25 August 2021 | Accepted: 26 August 2021

DOI: 10.1002/joc.7370

RESEARCH ARTICLE

International Journal of Climatology RMetS

Extreme precipitation variability across the Lancang-Mekong River Basin during 1952–2015 in relation to teleconnections and summer monsoons

Masoud Irannezhad[1] | Junguo Liu[1] | Deliang Chen[2]

[1]School of Environmental Science and Engineering, Southern University of Science and Technology, Shenzhen, China

[2]Regional Climate Group, Department of Earth Sciences, University of Gothenburg, Gothenburg, Sweden

Correspondence
Junguo Liu, School of Environmental Science and Engineering, Southern University of Science and Technology, Shenzhen, 518055, China.
Email: liujg@sustech.edu.cn; junguo.liu@gmail.com

Funding information
High-level Special Funding of the Southern University of Science and Technology, Grant/Award Numbers: G02296302, G02296402; National Natural Science Foundation of China, Grant/Award Number: 41625001; Strategic Priority Research Program of the Chinese Academy of Sciences, Grant/Award Number: XDA20060401; Swedish STINT, Grant/Award Number: CH2019-8377; Ministry of Science and Technology

Abstract

The Lancang-Mekong River Basin (LMRB) is home to ~70 million people whose life and livelihood are mostly dependent upon precipitation as the primary freshwater source. Hence, identifying potential oceanic–atmospheric drivers of regional precipitation variability is becoming increasingly important for the sustainable development of the LMRB. This study first investigated spatio-temporal variability and trends in extreme precipitation characteristics (in terms of intensity, frequency, and duration) throughout the LMRB during 1952–2015, using gauge-based gridded daily precipitation time series. Then, the associations between the historical extreme precipitation characteristics and seven teleconnection and five summer monsoon indices were explored. On the basin scale, no statistically significant ($p < .05$) trends were detected in annual extreme precipitation intensity, frequency, and duration indices. The number of wet days (R1mm) significantly increased in both the Mekong River Basin (MRB) and the Lancang River Basin (LRB), predominantly leading to longer wet spells in these two sub-basins. Spatially, the relatively high extreme precipitation intensity and frequency indices, as well as consecutive wet days (CWD), significantly increased in the south, east, and northwest of MRB, while decreased in the west of MRB and the north of LRB. The intensity and frequency of historical extreme precipitations over the LMRB were most significantly correlated with the East Asian Summer Monsoon Index, North Atlantic Oscillation, and East Pacific/North Pacific pattern. However, the wet/dry spells showed the strongest associations with the Atlantic Multi-decadal Oscillation/the Southern Oscillation Index on the interannual/decadal time scales (3–4/8–15 years) during 1986–1999/1968–2002, respectively.

KEYWORDS

APHRODITE, empirical orthogonal function (EOF), extreme precipitation, Lancang-Mekong River Basin, teleconnections, wavelet transform coherence (WTC)

 © 2021 Royal Meteorological Society

1 | INTRODUCTION

The global average air temperature significantly increased during 1880–2012, with a higher rate after 1975 (IPCC, 2013), mainly due to the substantial increases in atmospheric greenhouse gas concentrations (e.g., Zahn, 2009). Sea surface temperature (SST) has also warmed in recent decades because of considerable increases in global CO_2 concentration (Bâki Iz, 2018). According to the Clausius–Clapeyron (C–C) relationship, such warmer air and SST principally increase atmospheric moisture content (e.g., Bengtsson, 2010; Mishra *et al*., 2012; Ali and Mishra, 2017), and thereby significantly alter extremely high precipitation events worldwide (e.g., Myhre *et al*., 2019; Papalexiou and Montanari, 2019; Zhang and Zhou, 2019; Kirchmeier-Young and Zhang, 2020). These events have already posed different social, economic, and environmental challenges, particularly in developing countries due to high human density, vulnerable infrastructures, and poorly managed land use and development regulations (e.g., Yin *et al*., 2011; Liu *et al*., 2017).

On a global scale, both the intensity and frequency of extreme precipitation significantly increased in recent decades (Alexander *et al*., 2006; IPCC, 2013). Climate models also projected that such increases are very likely in the future, particularly during wet seasons (Kirtman *et al*., 2013; Collins *et al*., 2013; Rana *et al*., 2017) with higher water availability (Zhang and Zhou, 2019; Tabari, 2020). Such rising global extreme precipitation events, however, are not essentially translated to their similar changes on regional and local scales (Ramanathan and Feng, 2009; Xie *et al*., 2010; Westra *et al*., 2013). Accordingly, previous studies identified a large diversity in regional extreme precipitation around the world (e.g., Irannezhad *et* al., 2017; Mukherjee *et al*., 2018; Ohba and Sugimoto, 2019; Tabari *et al*., 2019; Bagtasa, 2020). In particular, Mainland Southeast Asia (MSA) as a wet tropical region with a complex distribution of land, sea, and terrain (Chang *et al*., 2005) as well as tremendous coastal human densities (World Bank, 2013) is highly vulnerable to the climate change impacts on extreme precipitation characteristics inducing disastrous consequences (e.g., Thi *et al*., 2012; Barros *et al*., 2014; Liu *et al*., 2015a). In this region, significant temperature warming has proportionally increased atmospheric water vapour (AWV), leading to more intense and frequent extreme precipitations, which can potentially enhance the already high risk of flood and drought in developing countries in MSA (IPCC, 2013; Barros *et al*., 2014).

The Lancang-Mekong River Basin (LMRB) is considered a home to about 70 million people from Vietnam, Cambodia, Thailand, Myanmar, Laos, and China (MRC, 2010), mostly (~80%) living close to the river (Ziv *et al*., 2012). About 40% of these residents are poor and typically working in primary freshwater-related sectors, particularly agriculture, forestry, and fishery (Dugan *et al*., 2010; MRC, 2010). As the key freshwater source, precipitation crucially contributes to the sustainable development in all six riparian countries the LMRB by supporting ecological environment protection, industrial and agricultural production, and regional socioeconomics (e.g., Choi *et al*., 2018). On the other hand, water-related natural hazards, particularly flood and drought, have significantly increased in the LMRB during recent decades (MRC, 2010; Räsänen *et al*., 2012; Pokhrel *et al*., 2018) mainly due to the alterations in regional extreme precipitation characteristics (IPCC, 2013; Phi Hoang *et al*., 2016; Ul Hasson *et al*., 2016). Causing fatalities and property damage, these hazards threaten persons living on the economic development margins in different parts of the LMRB (e.g., MRC, 2015). Accordingly, improving our knowledge on alterations in the spatio-temporal distribution of daily extreme precipitation across the LMRB can act towards achieving the United Nations' sustainable development goals (UN, 2015) in riparian countries.

Numerous factors can influence regional precipitation variability; including geographic characteristics (e.g., longitude, latitude, and altitude), large-scale oceanic–atmospheric teleconnections (e.g., the Atlantic Multi-decadal Oscillation or AMO), features of the climate system (e.g., the periodic climate fluctuation), solar radiation, human activities (e.g., anthropogenic sources of aerosol emissions), and so forth. (Ma *et al*., 2018). However, there exists controversy on the roles of such factors in extreme precipitation changes. Previous studies, for example, reported that more frequent extreme precipitation events, particularly extreme droughts (Zhang *et al*., 2017a) and heavy precipitation (Qian *et al*., 2009), were in response to the anthropogenic aerosols (Wang *et al*., 2019; Zhao *et al*., 2019; Tabari *et al*., 2020), while recent findings showed some robust repression/opposite effects of the aerosols (Lin *et al*., 2018). Meanwhile, spatial distribution of extreme precipitation characteristics (intensity, frequency, and duration) is generally controlled by various physical processes including moisture supply, uplift leading to condensation, evaporation or recycling, and water vapour flux divergence (e.g., Ma *et al*., 2020; Zhu *et al*., 2020; Liu *et al*., 2021). According to the water balance equation for atmosphere, changes in such processes are principally dependent upon (a) the exposure of study area to water vapour transport channel and source regions, (b) uplift of air mass by orography, atmospheric dynamics or thermal forcing, (c) surface water availability versus atmospheric evaporation demand relationship that can be composed to different energy and aerodynamic factors, and (d) wind velocity on the zonal and meridional directions (e.g., Liu *et al*., 2021). From a hydrological perspective, local precipitation characteristics are related to the moisture sources and transport pathways (e.g., Liu *et al*., 2021) driven by different oceanic–atmospheric circulations (e.g., Pathak *et al*., 2016; Jiang *et al*., 2017; Zhu *et al*., 2020).

Many previous studies already showed that atmospheric stability weakens as climate warming intensifies, leading to more intense and frequent precipitations over Southeast Asia (Sillmann *et al*., 2013; Donat *et al*., 2016). Across the LMRB, different predominant moisture sources (monsoons and mid-latitude westerlies) competitively influence precipitation characteristics, particularly during the summer (June–September) season (e.g., Turner and Annamalai, 2012; Misra and Dinapoli, 2014), in statistically significant ($p < .05$) association with the large-scale teleconnections (e.g., O'Gorman and Schneider, 2009; Delgado *et al*., 2012; Räsänen *et al*., 2016; Chen *et al*., 2019; Irannezhad *et al*., 2020) and summer monsoons (e.g., MRC, 2010; Delgado *et al*., 2012; Irannezhad *et al*., 2020). Accordingly, identifying the most influential teleconnections and/or summer monsoons for regional precipitation variability over the LMRB has been considerable debate in international research communities. Some scholars believe it is the El Niño-Southern Oscillation (ENSO; e.g., Villafuerte and Matsumoto, 2015), while some others mention the Western North Pacific Monsoon Index (WNPMI; e.g., Fan and Luo, 2019). Most of these previous studies, however, have measured the correlations of historical variations in precipitation and not extreme precipitations across the LMRB with one or a few climate teleconnections and/or summer monsoons, especially the ENSO. It is well motivated, hence, to comprehensively study the most significant teleconnections/summer monsoon indices influencing spatio-temporal variations in historical extreme precipitations throughout the LMRB.

In this article, we aimed at identifying teleconnections and/or summer monsoons affecting interannual extreme precipitation variability and trends across the LMRB during the water years (from November to the following October) over 1952–2015. Specific objectives were to (a) map historical climatologies of the extreme precipitations in the LMRB, (b) determine trends in such extreme precipitations over the study period (1952–2015), (c) identify the most dominant pattern of variations in regional extreme precipitations over time, and (d) explore and measure the relationships of historical extreme precipitations over the LMRB with teleconnections and summer monsoon indices.

2 | MATERIAL AND METHODS

2.1 | Study area

The Lancang-Mekong River (LMR; Figure 1a), with a drainage basin area of 795,000 km^2 and altitudes of 0–5,730 m (Figure 1b), is the world's 10th largest in terms of average annual outflow (475,000 m^3; e.g., Gupta, 2007; MRC, 2010). This river springs from the Tibetan Plateau (known as the world's Third Pole) in China, and then, runs through Myanmar, Laos, Thailand, Cambodia,

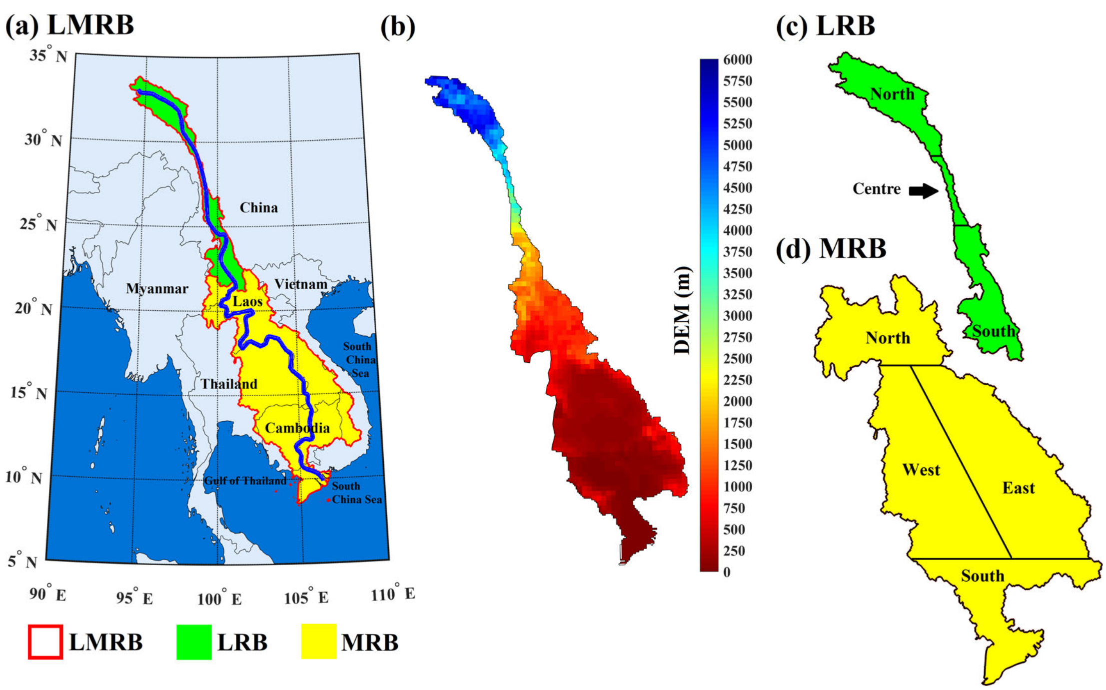

FIGURE 1 (a) The location of the Lancang-Mekong River Basin (LMRB), (b) its digital elevation model (DEM), (c) upper (Lancang River Basin or LRB), and (d) lower (Mekong River Basin or MRB) sections [Colour figure can be viewed at wileyonlinelibrary.com]

TABLE 1 Definitions of precipitation indices and their corresponding periods over which the teleconnections and summer monsoons were considered

						Corresponding period of	
Characteristic	**No.**	**ID**	**Indicator name**	**Description**	**Units**	**Teleconnections**	**Monsoons**
Intensity	1	R95p	Very wet days precipitation	Total precipitation from daily precipitation ≥95th percentile for 1951–2015	mm	Wet season (June–October)	Summer (June–September)
	2	R99p	Extremely wet days precipitation	Total precipitation from daily precipitation ≥99th percentile for 1951–2015	mm	Wet season (June–October)	
	3	RX1day	Maximum 1-day precipitation	Maximum 1-day precipitation	mm	Wet season (June–October)	
Frequency	4	R1mm	Number of wet days	Number of wet days (daily precipitation ≥1 mm)	Days	Water year (November–October)	
	5	R10mm	Heavy precipitation days	Number of days when daily precipitation ≥10 mm	Days	Wet season (June–October)	
	6	R20mm	Very heavy precipitation days	Number of days when daily precipitation ≥20 mm	Days	Wet season (June–October)	
Duration	7	CWD	Maximum length of wet spell	Maximum number of consecutive wet days (daily precipitation ≥1 mm)	Days	Wet season (June–October)	
	8	CDD	Maximum length of dry spell	Maximum number of consecutive dry days (daily precipitation <1 mm)	Days	Dry season (November–May)	

Mekong Delta in Vietnam, and then, discharges into the South China Sea. The LMRB is divided into two parts: (a) the upper (Lancang River Basin or LRB) (Figure 1c) and (b) the lower (Mekong River Basin or MRB) (Figure 1d). Across the LMRB, climate variability is strongly affected by the Indian Summer Monsoon (ISM), the East Asian Monsoon (EAM), and the Tropical Cyclones (TCs) MRC, 2010; Delgado *et al*., 2012;Chen *et al*., 2019). In general, the ISM conveys considerable moisture from the Indian Ocean towards the LMRB in the wet season (Jun–October), contributing about 70% to the annual precipitation. During the dry season (November–May), however, the EAM with high-pressure systems covers the LMRB (MRC, 2010; Delgado *et al*., 2012). The TCs also play a role in annual precipitation variability over the LMRB by influencing extreme precipitations (Chen *et al*., 2019). Long-term (1981–2010) average values for annual total precipitation show increases from the northwest of LRB (464 mm) to the east and southeast of MRB (4,300 mm). However, the temperature is consistently high across the MRB, while moderate throughout the LRB basically because of the higher elevations (Lutz *et al*., 2014). Accordingly, the annual mean temperatures ranged from −4.8°C across the LRB to 29.0°C in the southwest of the MRB for the period 1981–2010 (Lutz *et al*., 2014).

2.2 | Daily precipitation time series

For the LMRB, inadequate and irregular distribution of measurement stations limits monitoring spatio-temporal variations in precipitation (Wang *et al*., 2016). Such in-situ precipitation records are also discontinuous and uncertain as well as not even readily available, referring principally to various transboundary conflicts among all the six riparian countries in utilizing available freshwater resources in the basin (Lutz *et al*., 2014; Villafuerte and Matsumoto, 2015). Hence, previous studies have focused on using gauge-based gridded precipitation datasets in characterizing extreme precipitations over Southeast Asia (Sun *et al*., 2018; Yatagai *et al*., 2009, 2012; Villafuerte and Matsumoto, 2015), covering the LMRB (Ono *et al*., 2013; Lutz *et al*., 2014). Similarly, this study extracted high-resolution (0.25° × 0.25°), gauge-based, gridded daily precipitation data over the LMRB for 1951–2015 from the Asian Precipitation-Highly

Resolved Observational Data Integration Towards Evaluation (APHRODITE) product (Yatagai *et al.*, 2009, 2012), which is the only available long-term regional gauge-based daily gridded precipitation dataset for Asia (Tanarhte *et al.*, 2012). APHRODITE has been frequently used as a "ground truth" or "reference data" to assess the reliability of reanalysis and satellite-related precipitation datasets in Asia (e.g., Sidike *et al.*, 2016; Tan *et al.*, 2017), covering the LMRB (e.g., Chen *et al.*, 2018). Lutz *et al.* (2014) also recommended the APHRODITE for evaluating variability and trends in precipitation over the MRB in recent decades.

2.3 | Extreme precipitation indices

The Expert Team on Climate Change Detection and Indices defined and recommended a set of indices for identifying extreme precipitations around the world (Alexander *et al.*, 2006; Zhang *et al.*, 2011). This study selected eight of these indices to characterize the extreme precipitations throughout the LMRB during the water years (from November to following October) 1952–2015. The focus is put on characteristics of intensity, frequency, and duration of extreme precipitations. Table 1 gives key information about the 10 extreme precipitation indices employed by this study.

A few studies have already reported high uncertainty in the calculation of very wet days (R95p) (ID No. 1 in Table 1; e.g., Zolina *et al.*, 2009; Leander *et al.*, 2014). As an alternative, Zolina *et al.* (2009) suggested calculating the R95tt index defined as the fractional contribution of very wet days (R95p) to the total amount of precipitation from the probability distribution of daily precipitation. Comparing this index (R95tt) with S95pTOT developed based on individual 95th percentile value for each year, Leander *et al.* (2014) concluded that R95tt is principally more accurate than S95pTOT. The R95tt is also more stable for detecting very wet days at both seasonal and monthly scales, while practically consistent with the R95p index for evaluating changes in annual values of daily precipitation time series (Zolina *et al.*, 2009). Hence, we preferred to apply the R95p index (ID No. 1 in Table 1) for identifying annual very wet days throughout the LMRB in the water years (November–October) 1952–2015.

2.4 | Teleconnections and summer monsoons

Based on the current understanding of important teleconnections for regional climate variability (e.g., Ding *et al.*, 2019; Irannezhad *et al.*, 2020), this study selected seven large-scale teleconnection (Nos. 1–7 in Table 2) and five summer (June–September) monsoon (Nos. 8–12 in Table 2) indices. The monthly time series (1951–2015) for all these seven teleconnections and five summer monsoons were obtained from different sources given in Table 2. For the teleconnections (Nos. 1–7 in Table 2), this study calculated annual (as water year from November to following October) and seasonal (dry: November–May and wet: June–October) time series for the period 1952–2015 as the average of their monthly values. Accordingly, the water year 1952 (November 1951–October 1952) includes both dry (November 1951–May 1952) and wet (June 1952–October 1952) seasons of 1952.

2.5 | Statistical and analytical methods

The Mann-Kendall (MK) nonparametric test (Mann, 1945; Kendall, 1975) was used to detect statistically significant ($p < .05$) trends in different extreme precipitation indices. To estimate the slope of such statistically significant trends, the Sen method (Sen, 1968) was used. For measuring correlations of extreme precipitation indices with teleconnections and summer monsoons, the Spearman's rank correlation (ρ) rather than the Pearson's correlation coefficient (r) was used. The main reason for this choice is that the ρ, unlike the r, does not need to assume any particular distribution functions for the variables studied (Helsel and Hirsch, 1992). In the presence of positive serial correlations in extreme precipitation indices, teleconnections, or summer monsoons, we used (a) the trend-free prewhitening (TFPW) technique developed by Yue *et al.* (2002) to identify significant trends, and (b) the residual bootstrap (RB) approach developed by Park and Lee (2001) with 5,000 independent duplications to assess the standard deviation of the ρ values. For detecting statistically significant trends, the TFPW procedure only eliminates lag-one serial correlation in time series, while their autocorrelations might be up to several lags (Yue *et al.*, 2002). However, Bayazit and Önöz (2007) concluded that such serial correlations have negligible effects on the detection of significant trends in data sets with large samples ($n \geq 50$), like the time series employed by the present study. Both TFPW and RB methods have already been applied by previous studies for exploring variability and trends in extreme precipitation indices in different parts of the world (e.g., Irannezhad *et al.*, 2016; Dong *et al.*, 2019).

To identify and extract the spatial and temporal patterns (e.g., Hannachi *et al.*, 2007; Irannezhad *et al.*, 2020) of historical extreme precipitation indices throughout the LMRB, this study employed the empirical orthogonal function (EOF; Lorenz, 1956). Through the estimation of

TABLE 2 Summary of teleconnection and summer monsoon indices used

No.	Teleconnection or summer monsoon	ID	Reference	Data source
1	Atlantic Multi-decadal Oscillation	AMO	Enfield *et al.* (2001)	[a]NOAA Physical Sciences Division (PSD)
2	Arctic Oscillation	AO	Thompson and Wallace (1998)	NOAA Climate Prediction Centre (CPC)
3	East Pacific/North Pacific	EP/NP	Barnston and Livezey (1987)	NOAA climate prediction centre (CPC)
4	North Atlantic Oscillation	NAO	Barnston and Livezey (1987)	NOAA Climate Prediction Centre (CPC)
5	Pacific Decadal Oscillation	PDO	Zhang and Levitus (1997)	National Centre for Atmospheric Research (NCAR)
6	Southern Oscillation Index	SOI	Trenberth (1984)	National Centre for Atmospheric Research (NCAR)
7	Tibetan Plateau Index	TPI	Yao and Chen (2015)	National Climate Centre (NCC) of CMA[b]
8	Indian Summer Monsoon Index	ISMI	Wang and Fan (1999)	Asia-Pacific Research Data Centre (APRDC) of IPRC[c]
9	Western North Pacific Monsoon Index	WNPMI	Wang *et al.* (2001)	Asia-Pacific Research Data Centre (APRDC) of IPRC
10	East Asian Summer Monsoon Index	EASMI	Wang *et al.* (2008)	(http://ljp.gcess.cn/dct/page/65544)[d]
11	South Asian Summer Monsoon Index	SASMI	Li and Zeng (2002, 2003)	(http://ljp.gcess.cn/dct/page/65544)
12	South China Sea Summer Monsoon Index	SCSMI	Li and Zeng (2002, 2003)	(http://ljp.gcess.cn/dct/page/65544)

[a]NOAA (National Oceanic and Atmospheric Administration of the United States).
[b]CMA (China Meteorological Administration).
[c]IPRC (International Pacific Research Centre).
[d]Last accessed 7 April 2020.

EOFs, the North criterion significance test (North *et al.*, 1982) was also used to differentiate between the physical signal and the noise. Besides, the leading PCs were designated as the substitutions to measure the relationships of annual extreme precipitation indices over the LMRB with different teleconnections and summer monsoons.

In recent years, the wavelet transform coherence (WTC) method has been employed by several studies for identifying the potential drivers of regional climate variability in the time–frequency domain at different time steps (e.g., Asong *et al.*, 2018; Fang *et al.*, 2019; Irannezhad *et al.*, 2020). Hence, this study used this method (WTC) to explore significant ($p < .05$) associations of the dominant EOFs of annual extreme precipitation indices in the LMRB with teleconnections and summer monsoons. As a new signal-analysis technique, the WTC method is a combination of both wavelet transform and cross-spectrum analyses. Thus, this method (WTC) measures the degree of possible linearity between two non-stationary time series in both time and frequency domains (Jiang *et al.*, 2019; Su *et al.*, 2019). The significance level of WTC is calculated by the Monte–Carlo method considering only values outside of the cone-of-influence (Torrence and Compo, 1998; Grinsted *et al.*, 2004).

3 | RESULTS

3.1 | Trends in annual extreme precipitation indices during 1952–2015

On the basin scale, statistically significant ($p < .05$) trends in R95p (−0.68 mm·decade^{-1}), R1mm (0.19 days·decade^{-1}), and CWD (0.42 days·decade^{-1}) reflect less intense very wet day precipitation, more frequent wet days, and longer wet spells, respectively, across the LRB (Figure 2a–c). Similar to the LRB, the number of wet days and the length of wet spells increased across the MRB, referring in turn to the significant trends in the R1mm (0.325 days·decade^{-1}) and the CWD (0.46 days·decade^{-1}) indices (Figure 2d,e). However, no statistically significant trends were found in annual extreme precipitation indices across the LMRB (Table 3).

All extreme precipitation intensity indices (Nos. 1–3 in Table 1) significantly ($p < .05$) increased in 16.1–28.5% of grids throughout small parts in the south, southeast, and northwest of MRB; while decreased in 4.7–15.9% of grids over some areas in the west of MRB as well as the south and north of the LRB (Figure 3a–c). The highest rate of such an increasing (decreasing) trend was about 93.8 (−50), 48 (−32), and 6 (−6) mm decade^{-1} for R95p, R99p, and RX1day, respectively (Figure 3a–c). Regarding the frequency of extreme precipitations, all R1mm, R10mm, and R20mm indices showed significant increases (decreases) in 32.5–38.5% (5.9–12.9%) of grids throughout LMRB, mainly found over the north and southeast (west) of MRB (Figure 3d–f). Grids with significant increases in both R10mm and R20mm were also seen in the south of LRB (Figure 3e,f). Besides, R1mm (R10mm) showed grids with significant increases (decreases) throughout the LRB (Figure 3d,e). The rates for such trends throughout the LMRB ranged between −7 and 9, −3 and 4.5, and −1.5 and 3 (day decade^{-1}) for R1mm, R10mm, and R20mm, respectively (Figure 3d–f). Statistically significant trends in CWD (Figure 3g) mostly (21.8% of grids) determined longer wet spells particularly over the east of MRB and some parts in the west of MRB, with the highest rate of 8.4 (day decade^{-1}). Interestingly, longer dry spells were also observed in 9.3% of grids seen over small areas in the east of MRB and the south of LRB, with the highest rate of 8.5 (day decade^{-1}) (Figure 3h).

3.2 | Dominant patterns of historical extreme precipitation variability

The historical variations in annual extreme precipitation indices were generally higher in the MRB than those in the LRB (Table 3). Compared to the LRB, the MRB has also experienced more intense, more frequent,

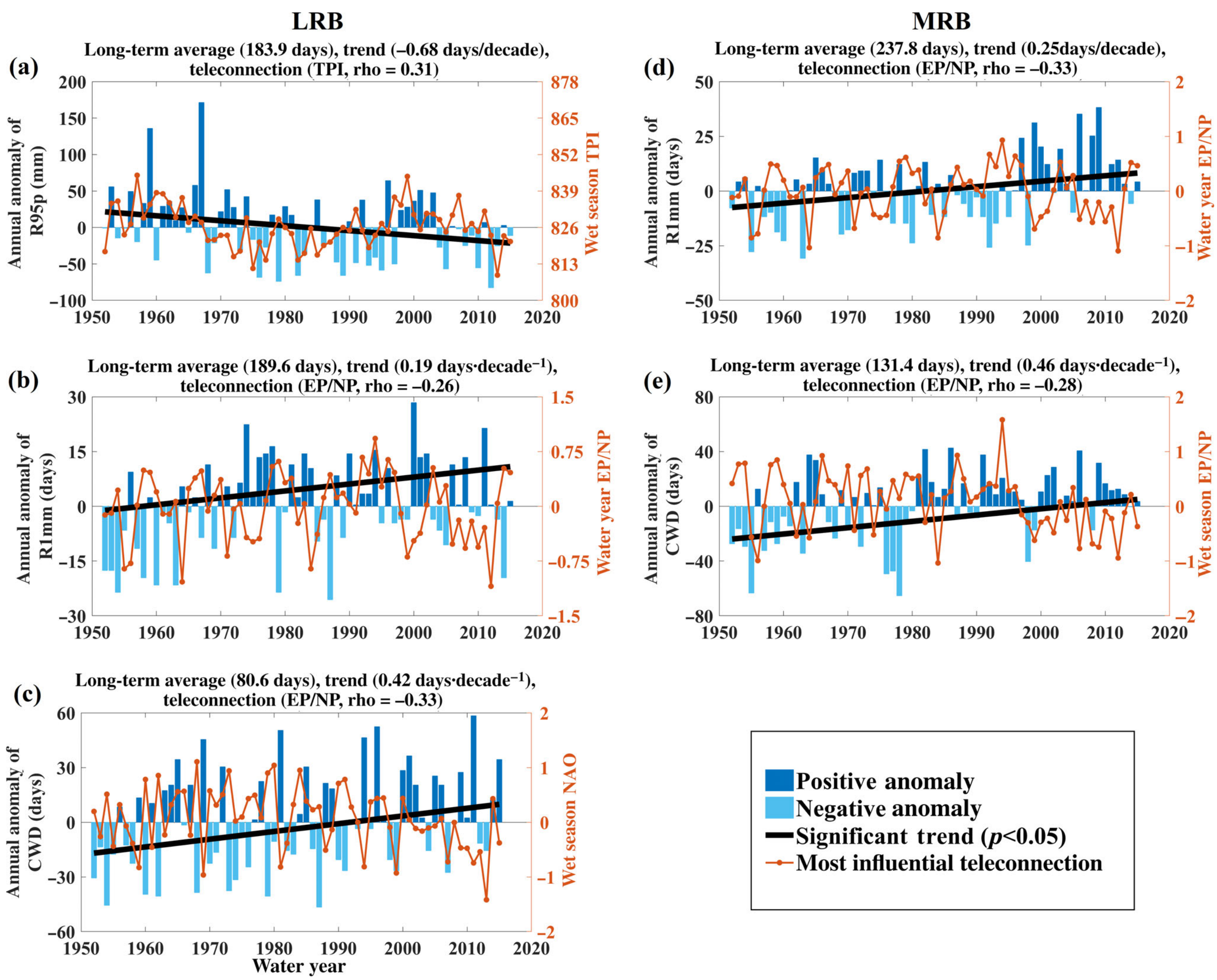

FIGURE 2 Time series with trend line and most significant teleconnection or summer monsoon for (a) R95p, (b) R1mm, and (c) CWD over the LRB; and for (d) R1mm and (e) CWD over the MRB, during the water years (November–October) 1952–2015 [Colour figure can be viewed at wileyonlinelibrary.com]

TABLE 3 Statistically significant ($p < .05$) trend (/decade), variability, most significant correlations (rho, $p < .05$) with teleconnections or summer monsoons, and percentage of variance explained by the first three varimax loadings (empirical orthogonal functions, EOFs) for the selected annual extreme precipitation indices (Table 1) across the LMRB, LRB, and MRB during the water years (November–October) 1952–2015

Basin	Extreme Precipitation Index (unit)	Significant trend (/decade, $p < .05$)	Minimum	Maximum	Long-term average	Most significant teleconnection or summer monsoon (rho, $p < .05$)[a]	Empirical orthogonal functions (EOFs)		
							EOF_1 (%)	EOF_2 (%)	EOF_3 (%)
LRB	R95p (mm)	−0.68	101.2	355.3	183.9	TPI (0.31)	32.6	14.9	10.4
	R99p (mm)		0.0	172.9	50.5	SASMI (0.25)	26.8	17.4	10.7
	RX1day (mm)		10.5	23.4	15.3	WNPMI (−0.34)	27.1	16.7	16.7
	R1mm (days)	0.19	164	218	189.6	EP/NP (−0.26)	33.2	23.8	12.4
	R10mm (days)		1.0	20.0	7.1	TPI (0.29)	39.5	12.3	7.9
	R20mm (days)		0.0	1.0	0.1		31.9	14.8	9.8
	CWD (days)	0.42	34.0	139.0	80.6	NAO (−0.33)	29.6	13.5	7.4
	CDD (days)		22.0	83.0	40.9	TPI (0.26)	26.8	12.6	10.4
MRB	R95p (mm)		116.8	509.4	267.1	TPI (0.30)	16.1	11.6	7.3
	R99p (mm)		0.0	224.8	71.7		17.3	8.8	7.1
	RX1day (mm)		15.1	38.4	22.1	NAO (0.29)	18.5	10.2	6.9
	R1mm (days)	0.25	207.0	276.0	237.8	EP/NP (−0.33)	38.1	15.8	11.6
	R10mm (days)		13.0	53.0	31.1	AMO (+0.32)	22.6	11.2	9.4
	R20mm (days)		0.0	7.0	1.2	EASMI (−0.26)	15.2	10.7	7.5
	CWD (days)	0.46	66.0	174.0	131.4	EP/NP (−0.28)	16.5	11.5	6.6
	CDD (days)		19.0	86.0	41.2	AMO (−0.27)	22.6	16.1	6.8
LMRB	R95p (mm)		84.4	395.7	215.2	EASMI (0.29)	15.2	10.7	7.6
	R99p (mm)		0.0	195.5	55.6		16.3	8.6	6.8
	RX1day (mm)		12.1	27.3	17.1	NAO (0.27)	18.4	10.3	6.7
	R1mm (days)		203.0	266.0	231.2	EP/NP (−0.32)	33.2	14.1	9.9
	R10mm (days)		5.0	29.0	15.3	EASMI (0.33)	20.6	10.5	8.9
	R20mm (days)		0.0	1.0	0.2		14.7	9.9	7.5
	CWD (days)		94.0	168.0	137.1	SOI (0.25)	14.5	10.9	7.1
	CDD (days)		18.0	89.0	46.1		17.4	12.6	8.2

[a]Strongest (most) significant correlation: the highest absolute Spearman's rank correlation at 5% significance level ($p < .05$).

and longer extreme precipitations during the water years 1952–2015 (Table 3). About 50–70% (33–65%) of the total variance in annual extreme precipitation indices across the LRB (MRB) were reflected in their first three EOFs (Table 3). However, the first EOF or EOF_1 of annual extreme precipitation indices were approximately 1.4–3.2 (1.6–5.0), 1.4–2.4 (2.0–3.3), and 1.3–2.4 (2.0–3.4) times greater than those of the second EOF or EOF_2 (the third EOF or EOF_3) over the LRB, MRB, and LMRB, respectively (Table 3). As the most important patterns of annual extreme precipitation indices across the LMRB, these EOF_1 were used for subsequent analysis and discussion in the present study. The same analyses for both EOF_2 and EOF_3 are given in the Supporting Information. Accordingly, historical variations in annual extreme precipitations across the MRB (with EOF_1 between 15.2 and 38.1%) are more complex to explain than those across the LRB (with EOF_1 between 26.8 and 39.5%; Table 3).

Based on spatial analyses, the range of variability was 120–920 mm for R95p, 30–300 mm for R99p, 10–110 mm for RX1day, 90–230 days for R1mm, 0–100 days for R10mm, 0–50 mm for R20mm, 12–52 days for CWD, and 15–103 days for CDD across the LMRB through the water years 1952–2015 (Figure 4). In general, relatively high (low) intensity and frequency extreme precipitation indices as well as longer (shorter) wet and shorter (longer) dry spells were typically seen over the east and southeast

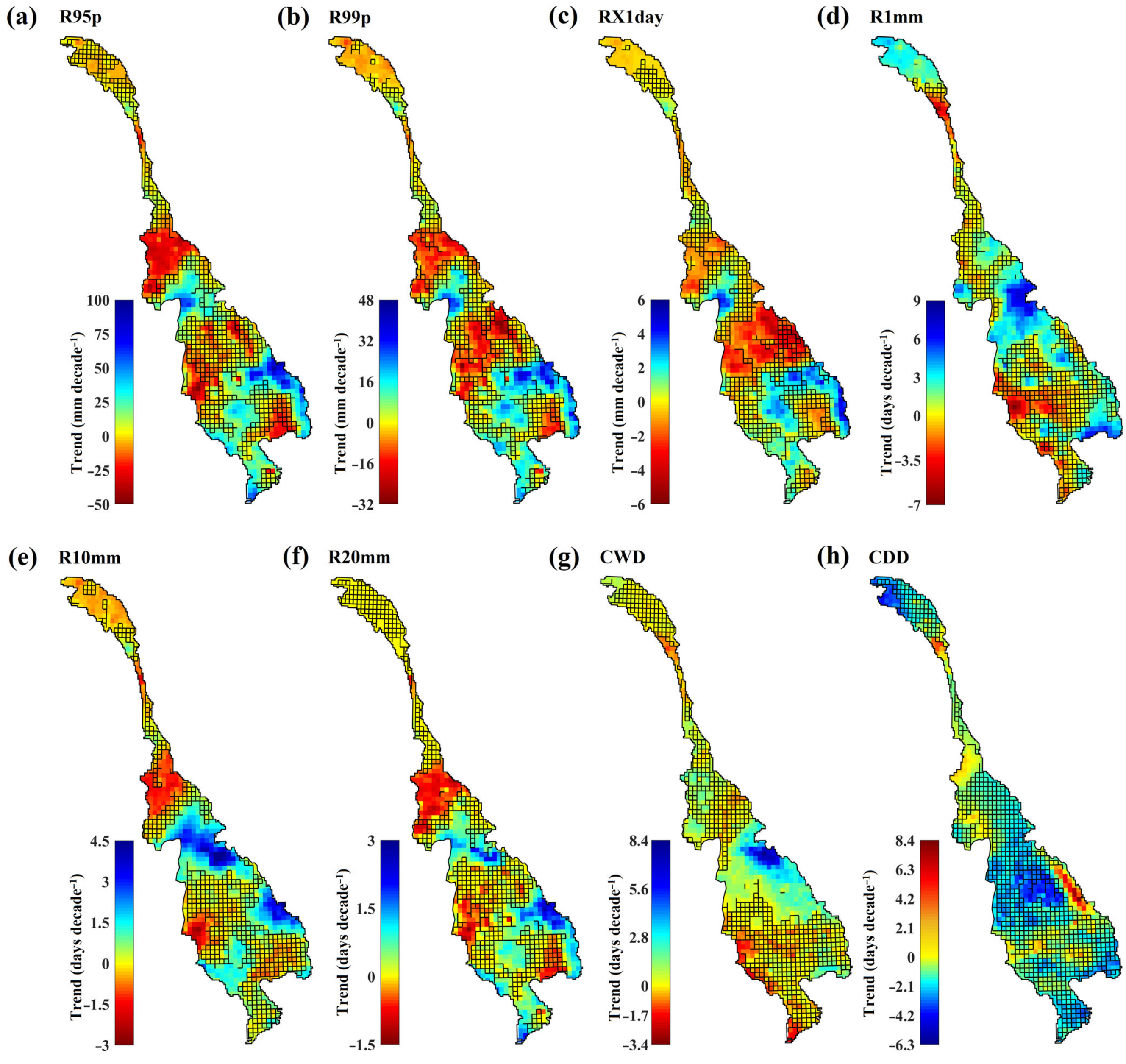

FIGURE 3 Spatial distribution maps of trends in (a) R95p, (b) R99p, (c) RX1day, (d) R1mm, (e) R10mm, (f) R20mm, (g) CWD, and (h) CDD, throughout the LMRB during the water years (November–October) 1952–2015. The stippling indicates areas where the trends are statistically insignificant ($p > .05$) [Colour figure can be viewed at wileyonlinelibrary.com]

of MRB (the north of LRB; Figure 4). Such patterns were also reflected in the spatial distribution maps of EOF_1 for annual extreme precipitation indices throughout the LMRB during the water years 1952–2015 (Figure 5) Accordingly, these $EOFs_1$ identified strong negative (positive) centres for R95p, R99p, R20mm, CWD, and CDD (RX1day, R1mm, and R10mm) over the east and southeast of MRB (Figure 5). A strong positive centre was also found in the northeast of MRB for the R10mm (Figure 5e), in the west of MRB for the R1mm (Figure 5d), and in the most northern part of the LRB for the CDD (Figure 5h).

3.3 | Influential teleconnections and summer monsoons

Teleconnections and summer monsoons showed significant correlations (Table 4) not only with each other but also with different extreme precipitation indices (Figure 6). In the LRB, the TPI, EP/NP, and NAO were the strongest teleconnections associated with historical year-to-year variations in R95p (ρ = 0.31), R1mm (ρ = −0.26) and CWD (ρ = −0.33), respectively (Figure 6a). In this basin (LRB), the TPI was also the most significant teleconnection positively correlated with

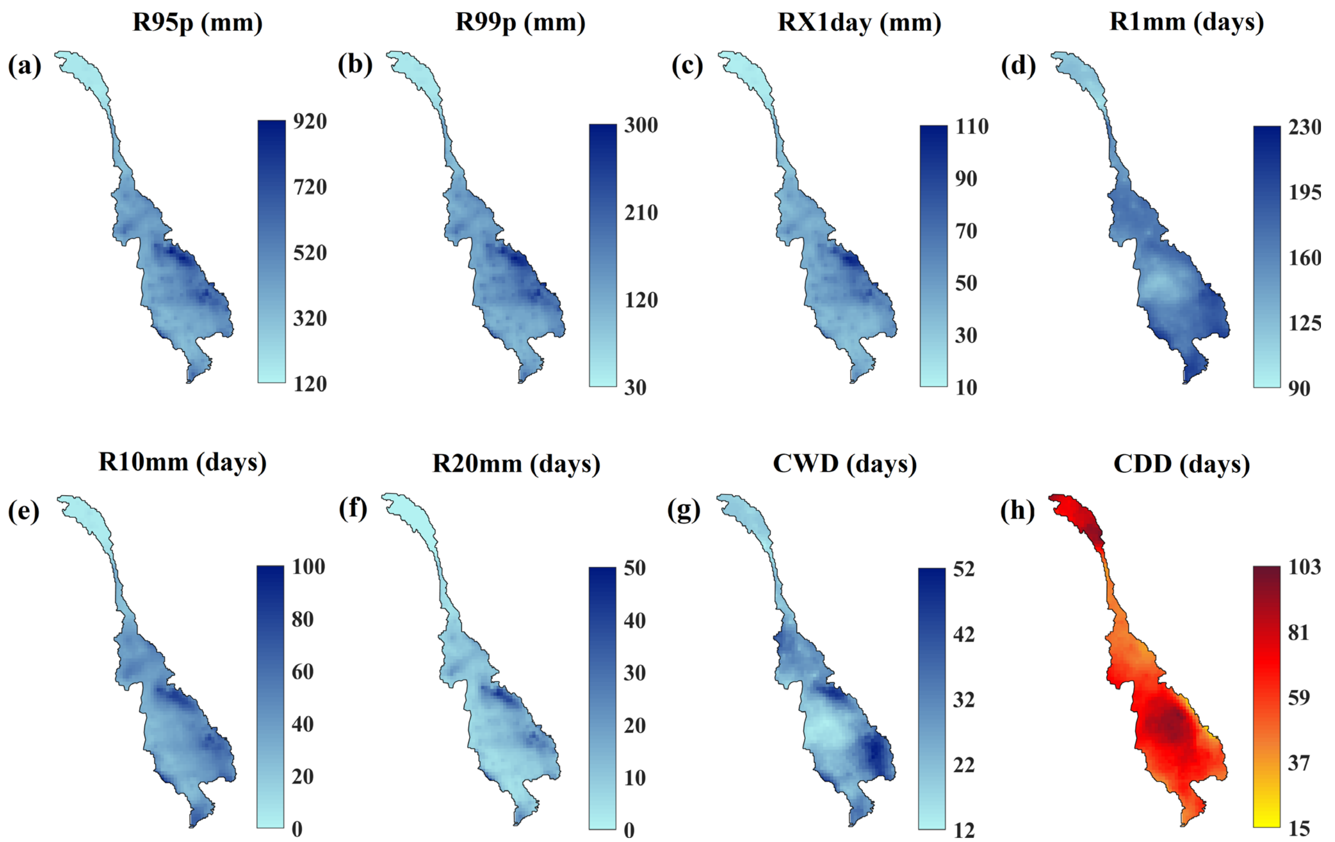

FIGURE 4 Spatial distribution maps of long-term average values for (a) R95p, (b) R99p, (c) RX1day, (d) R1mm, (e) R10mm, (f) R20mm, (g) CWD, and (h) CDD, throughout the LMRB during the water years (November–October) 1952–2015 [Colour figure can be viewed at wileyonlinelibrary.com]

the historical variations in both R10mm and CDD (Figure 6a). Besides, the relatively high extreme precipitation index of R99p (RX1day) in the LRB showed the strongest positive (negative) relationships with the SASMI (WNPMI) in recent decades, with $\rho = 0.25$ (-0.34) (Figure 6a). Besides, the WNPMI and the SASMI were also the influential summer monsoons for inter-annual variability in CWD and R10mm over the LRB, respectively (Figure 6a).

In the MRB, year-to-year variations in both R1mm and CWD were most strongly connected to the EP/NP, while in both R10mm and CDD to the AMO (Figure 6b). This teleconnection (AMO) also showed significant relationships with R95p ($\rho = 0.27$) and R1mm ($\rho = 0.28$) in the MRB (Figure 6b). Moreover, historical variations in R95p, RX1day, and R20mm across the MRB were most significantly associated with the TPI, NAO, and EASMI, respectively (Figure 6b). In the MRB, the ISMI, WNPMI, and EASMI were the influential summer monsoons for historical extreme precipitation variability (Figure 6b).

Similar to both LRB and MRB, the EP/NP showed the most significant correlation ($\rho = -0.32$) with the number of wet days (R1mm) over the LMRB (Figure 6c). In this basin (LMRB), the EASMI was the most influential summer monsoon for year-to-year historical variations in both R95p and R10mm (Figure 6c), which were also significantly correlated with the TPI (Figure 6c). Besides, RX1day and CWD were most significantly associated with the NAO and the SOI, respectively (Figure 6c). Moreover, the SOI (EP/NP) showed significant positive (negative) relationships with the R1mm (CWD) across the LMRB in recent decades (Figure 6c).

The AMO, PDO, NAO, and TPI were the key common teleconnections most significantly influencing extreme precipitation intensity indices (R95p, R99p, and RX1day) throughout the LMRB (Figure 7). Such relationships were: (a) positive with the AMO mainly seen in the north of MRB; (b) positive with PDO in the south, southeast, and east of MRB; and (c) negative with the NAO across the north of LRB and some parts in the east and west of MRB. The number of wet days (R1mm) showed the strongest correlations with: (a) the AMO over the south and west of MRB as well as the north of LRB; (b) the PDO in the southwest and north of MRB; and (c) the EP/NP some parts in the west, east and north of MRB (Figure 7d,h). The most significant relationships of

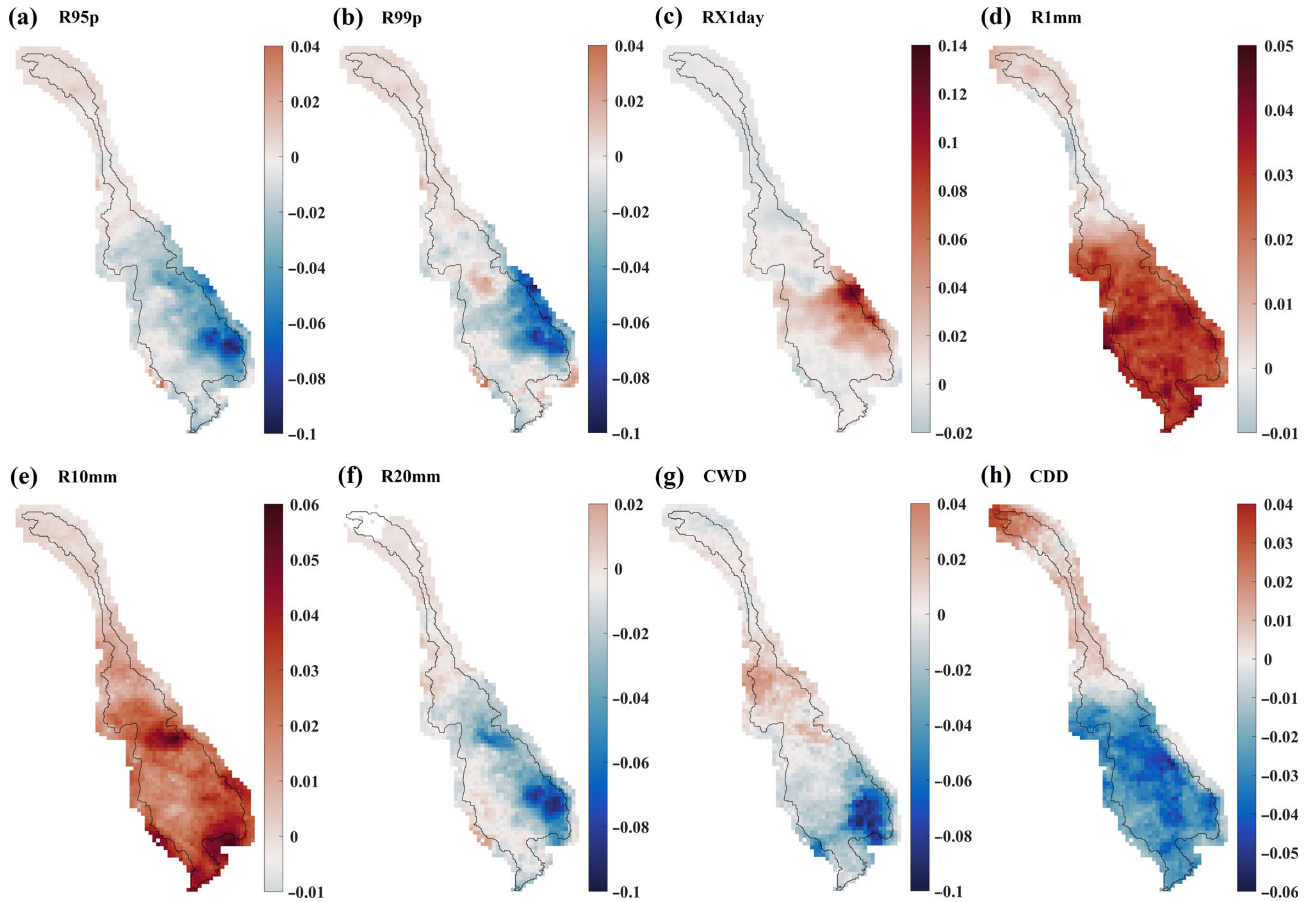

FIGURE 5 Spatial patterns of the first mode of empirical orthogonal function (EOF_1) for (a) R95p, (b) R99p, (c) RX1day, (d) R1mm, (e) R10mm, (f) R20mm, (g) CWD, and (h) CDD, throughout the LMRB during the water years (November-October) 1952–2015 [Colour figure can be viewed at wileyonlinelibrary.com]

TABLE 4 Spearman's rank correlations among historical (1952–2015) wet season' teleconnections and summer monsoons considered by this study

	NAO	EP/NP	AO	PDO	SOI	AMO	TPI	ISMI	WNPMI	EASMI	SASMI	SCSMI
NAO	**1.00**											
EP/NP	0.20	**1.00**										
AO	**0.48**	−0.22	**1.00**									
PDO	−0.04	**0.35**	**−0.31**	**1.00**								
SOI	−0.04	**−0.41**	**0.36**	**−0.46**	**1.00**							
AMO	**−0.29**	**−0.37**	0.09	**−0.30**	**0.33**	**1.00**						
TPI	−0.05	−0.18	0.09	−0.21	0.09	**0.26**	**1.00**					
ISMI	−0.02	**0.31**	**−0.30**	**0.27**	**−0.38**	−0.07	0.10	**1.00**				
WNPMI	−0.07	−0.11	0.02	−0.23	**0.29**	0.21	−0.06	−0.18	**1.00**			
EASMI	0.06	−0.08	0.04	−0.22	**0.26**	0.00	0.14	−0.13	**0.69**	**1.00**		
SASMI	0.06	0.13	−0.12	0.01	−0.14	−0.01	0.19	**0.69**	0.10	**0.25**	**1.00**	
SCSMI	0.06	0.11	0.04	−0.17	**0.29**	0.04	−0.01	−0.15	**0.75**	**0.73**	0.21	**1.00**

Note: In bold if statistically significant ($p < .05$).

R10mm with the AMO, PDO, and EASMI were found in the north, east, and south of MRB, respectively (Figure 8a,e). The R20mm was most commonly correlated with the SASMI over the south of MRB, and then, with the AMO across the north of MRB (Figure 8b, f). Extreme precipitation duration index of CWD was

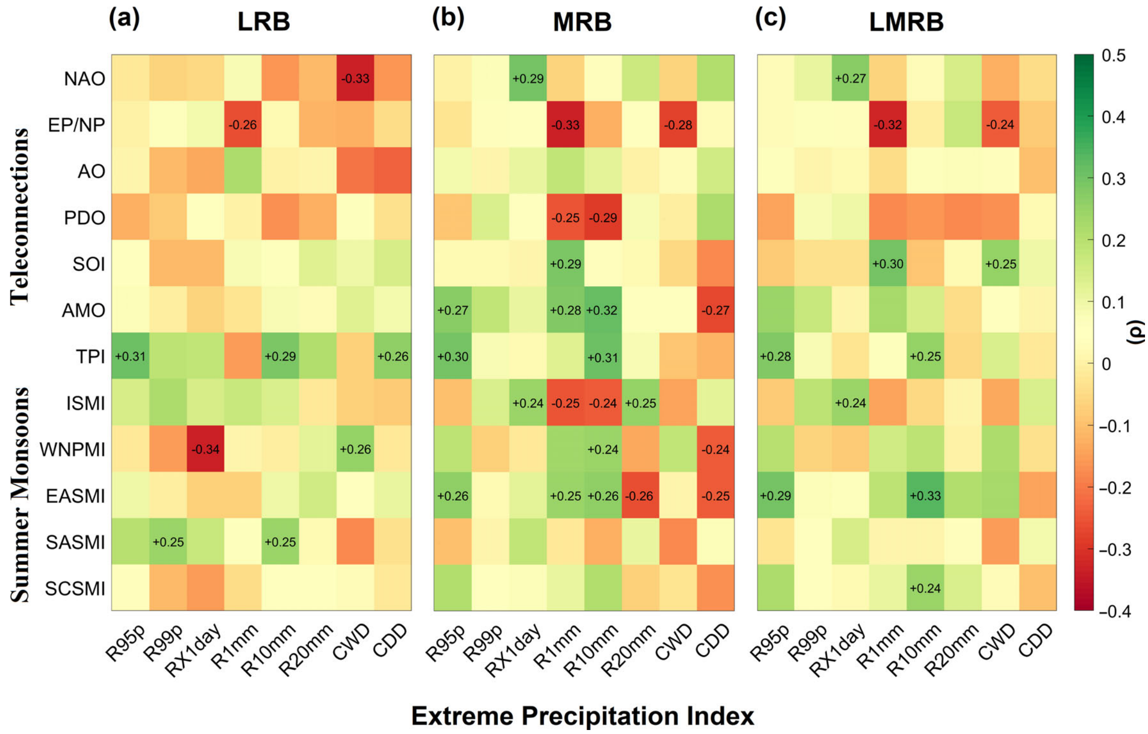

FIGURE 6 The Spearman's rank correlations (ρ) of extreme precipitation indices with teleconnections over (a) LRB, (b) MRB, and (j) LMRB, during the water years 1952–2015. The values show statistically significant ($p < .05$) correlations [Colour figure can be viewed at wileyonlinelibrary.com]

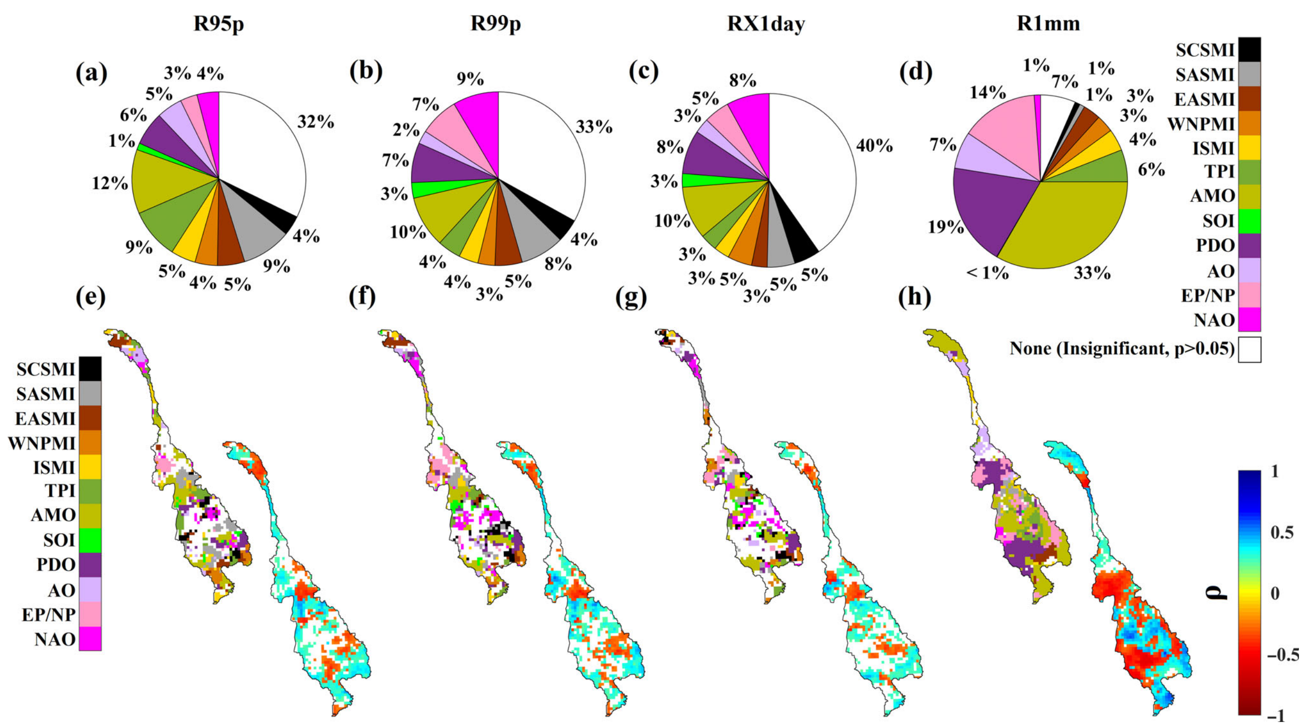

FIGURE 7 Percentage of most influential climate teleconnections (upper row) as well as spatial distribution maps (lower row) of their name (left) and Spearman rank correlation (right) with extreme precipitation indices of (a and e) R95p, (b and f) R99p, (c and g) RX1day, and (d and h) R1mm, throughout the LMRB during the water years 1952–2015 [Colour figure can be viewed at wileyonlinelibrary.com]

mainly associated with the PDO over the north of MRB, the TPI across the southwest of MRB, with the EP/NP at upper grids in the east and west of MRB, and with the SOI throughout the southeast of MRB (Figure 8c,g). Besides, the maximum length of dry spells (CDD) showed the strongest relationships mainly with the AMO, SOI, and EASMI in the southeast, southwest, and south of MRB, respectively (Figure 8d,h).

3.4 | Phase difference of extreme precipitation indices with teleconnections/summer monsoons

Table 5 gives Spearman's rank correlations (ρ) for the first three corresponding time coefficients (PCs) of annual extreme precipitation indices with teleconnections and summer monsoons throughout the LMRB during the water years (November–October) 1952–2015. However, this study only discussed the most significant relationships of the first PCs (PC_1s) of annual extreme precipitation indices with teleconnections and summer monsoons. Accordingly, the EASMI was the most influential summer monsoon for interannual variations in the first corresponding time coefficients (PC_1s) of R95p, R10mm, and R20mm throughout the LMRB in recent decades, while the NAO for the PC_1s of R99p and RX1day (Table 5). Besides, the PC_1s of R1mm, CWD, and CDD showed the strongest relationships with the EP/NP, SOI, and AMO, respectively (Table 5).

The PC_1 of R95p showed the significant coherence with the EASMI on the 1- to 4-year time scale during 1974–1986, with phase differences between −90 and −135° (Figure 9a), indicating that the EASMI was ahead of the R95p in the LMRB by 2–6 to 3–12 months, respectively (Table 6). Similarly, the lags of EASMI with the PC_1 of R10mm ranged from 0 (during 1959–1963, 1980–1985, and 2003–2012 on the time scales of 4–6, 3–6, and 1–7 years, respectively) to 1–2 (during 1965–1979 and 1995–1997 on the time scales of 4–5 and 1–2 years, respectively) months (Figure 9e and Table 6). On the interannual time scales of 6–8, 1–5, and 1–3 years, the EASMI also hindered the PC_1 of R20mm by 2–3, 1–8 to 3–15, and 1–3 months in 1959–1970, 1975–1980, 1994–1998, in turn (Figure 9f). Besides, the EASMI was the strongest summer monsoon simultaneously exerting negative influences on the PC_1 of R20mm on the time scale of 1–2 year(s) (Table 6).

On the time scale of 4–6 years, the NAO had a significant positive (negative) coherence with the PC_1 of R99p (RX1day) during 1959–1963 (1959–1961; Figure 9b,c), with the phase difference of −10° (100°) that indicates

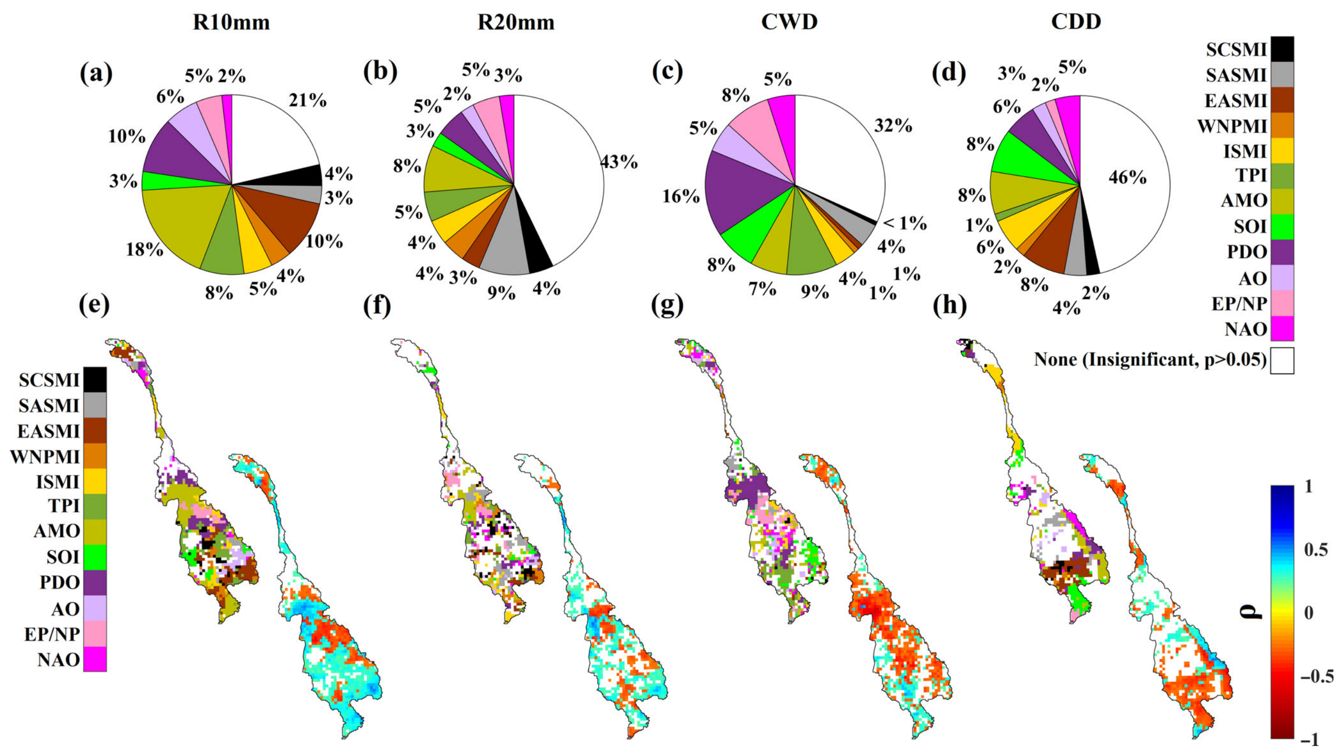

FIGURE 8 Percentage of most influential climate teleconnections (upper row) as well as spatial distribution maps (lower row) of their name (left) and Spearman rank correlation (right) with extreme precipitation indices of (a and e) R10mm, (b and f) R20mm, (c and g) CWD, and (d and h) CDD, throughout the LMRB during the water years 1952–2015 [Colour figure can be viewed at wileyonlinelibrary.com]

TABLE 5 Spearman's rank correlations (ρ) for the first three corresponding time coefficients (PCs) of annual extreme precipitation indices with teleconnections and summer monsoons throughout the LMRB during the water years (November–October) 1952–2015

		Teleconnection							Summer monsoon				
Basin	**Extreme Precipitation Index (unit)**	**NAO**	**EP/NP**	**AO**	**PDO**	**SOI**	**AMO**	**TPI**	**ISMI**	**WNPMI**	**EASMI**	**SASMI**	**SCSMI**
PC_1	R95p (mm)	−0.21	−0.05	−0.18	−0.04	0.01	0.06	−0.21	0.12	−0.21	**−0.26**	0.11	**−0.25**
	R99p (mm)	**−0.35**	−0.11	−0.19	−0.22	0.01	**0.27**	0.03	−0.02	0.01	−0.08	0.03	−0.05
	RX1day (mm)	**0.35**	0.05	**0.26**	0.08	0.11	−0.15	−0.06	0.01	0.01	0.08	−0.09	0.01
	R1mm (days)	**−0.25**	**−0.51**	0.01	**−0.48**	0.38	**0.49**	**0.26**	−0.11	0.11	**0.31**	0.08	0.16
	R10mm (days)	−0.07	−0.22	0.17	**−0.32**	0.18	**0.41**	**0.39**	−0.14	**0.28**	**0.42**	0.06	**0.31**
	R20mm (days)	−0.15	−0.02	−0.18	0.03	0.09	−0.01	**−0.25**	0.11	−0.22	**−0.27**	0.05	**−0.26**
	CWD (days)	−0.01	−0.18	0.11	−0.04	**0.35**	0.22	−0.13	−0.12	0.01	−0.16	−0.19	0.01
	CDD (days)	−0.18	−0.19	−0.08	**−0.32**	0.21	**0.36**	0.17	−0.11	0.12	0.21	−0.01	0.13
PC_2	R95p (mm)	−0.17	−0.21	0.06	**−0.26**	**0.38**	**0.45**	0.23	−0.17	**0.26**	**0.31**	0.04	**0.26**
	R99p (mm)	−0.01	−0.18	**0.26**	−0.19	**0.41**	**0.33**	0.07	**−0.31**	**0.32**	**0.32**	−0.12	**0.33**
	RX1day (mm)	−0.18	−0.15	0.13	−0.18	0.21	**0.26**	−0.05	−0.17	0.06	0.09	−0.08	0.03
	R1mm (days)	**0.25**	0.15	−0.02	0.12	0.02	0.11	0.05	−0.01	0.11	**0.26**	0.09	0.04
	R10mm (days)	0.07	−0.08	0.01	−0.14	−0.13	−0.05	0.11	−0.06	−0.01	0.01	−0.09	0.03
	R20mm (days)	−0.19	−0.18	0.01	−0.22	**0.31**	**0.28**	**0.26**	−0.11	0.21	**0.25**	0.05	0.18
	CWD (days)	0.01	0.21	−0.14	**0.44**	−0.16	−0.17	**−0.37**	0.18	−0.01	−0.07	0.13	0.03
	CDD (days)	0.05	−0.09	−0.11	−0.01	0.19	0.06	0.11	0.01	−0.02	0.16	0.09	−0.04
PC_3	R95p (mm)	−0.13	−0.18	−0.11	−0.18	0.07	0.15	0.06	−0.11	0.04	−0.04	−0.13	0.02
	R99p (mm)	**−0.26**	0.11	−0.22	0.13	−0.18	0.14	0.13	0.23	−0.03	−0.07	0.07	−0.02
	RX1day (mm)	0.12	−0.03	−0.04	−0.14	−0.11	−0.14	−0.18	0.04	−0.21	−0.12	−0.02	−0.21
	R1mm (days)	0.13	−0.07	−0.04	**0.26**	−0.07	0.02	0.13	**0.27**	−0.07	0.09	0.14	−0.09
	R10mm (days)	0.08	0.07	0.09	0.21	−0.09	−0.05	0.07	−0.09	0.07	0.18	−0.01	0.11
	R20mm (days)	−0.09	**−0.26**	−0.14	**−0.33**	0.08	0.12	0.13	−0.12	0.01	−0.04	−0.06	0.02
	CWD (days)	**−0.25**	−0.12	−0.07	**−0.24**	0.11	**0.32**	0.09	−0.11	0.02	−0.02	−0.05	0.08
	CDD (days)	0.11	−0.03	0.07	0.11	**−0.25**	−0.09	−0.06	**0.26**	−0.19	−0.16	0.01	−0.21

Note: In bold if statistically significant ($p < .05$).

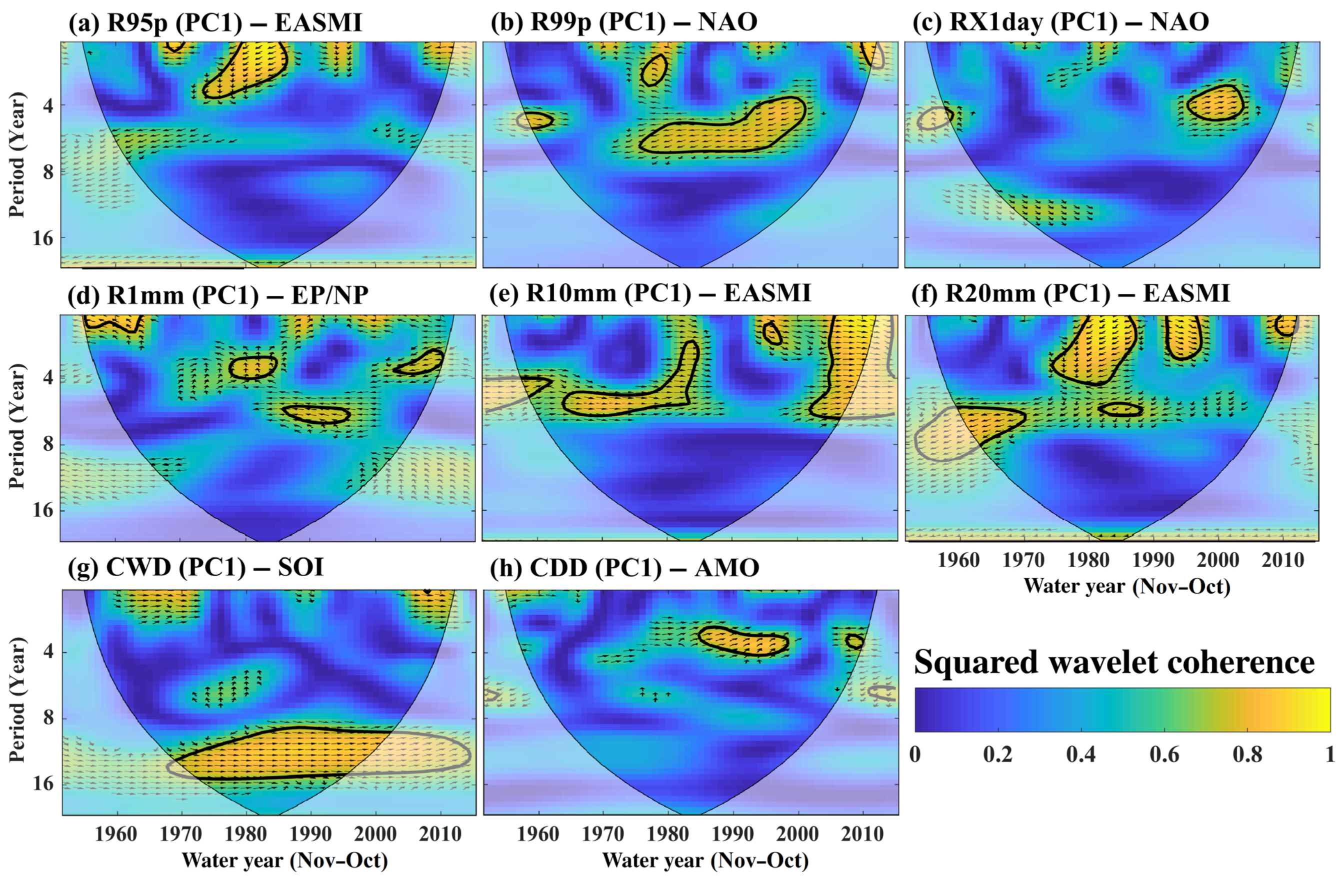

FIGURE 9 Wavelet transforms coherence and phase differences for the most significant teleconnection or summer monsoon and the first EOF (PC1) mode of the selected annual extreme precipitation indices over the Lancang-Mekong River Basin (LMRB) [Colour figure can be viewed at wileyonlinelibrary.com]

the NAO lagged (led) the R99p (RX1day) by 1–2 (11–16) months over the LMRB (Table 6). The PC_1 of R99p also exhibited significant negative relationships with the NAO on the interannual time scales of 4–8 and 1–2 years during 1978–2000 and 2009–2011 with the phase differences of −150° (the lag of 4–8 months) and 170° (the lead of 0–1 month), respectively (Figure 9b). The NAO was correspondingly the most influential teleconnection for the 1–2 months leading time of the PC_1 of RX1day on the time scale of 3–5 years during 1995–2005 (Table 6).

According to the strongest coherences, the number of wet days (R1mm) was negatively associated with the EP/NP on the interannual time scales of 1–2, 3–4, 6–8, and 3–4 years during 1954–1964, 1978–1983, 1984–1996, and 2004–2009, with the phase differences of 135°, 90–100°, 170°, and −150°, respectively (Figure 9d and Table 6). The AMO was the most influential teleconnection for the CDD variability over the LMRB on the interannual time scale of 3–4 years, with the 45° phase difference (lead of 4–6 months; Figure 9h). The CWD was the only extreme precipitation index that showed the strongest coherence with the SOI on the decadal time scale of 8–15 years during 1968–2002, with the phase difference of 0° (simultaneous) (Figure 9g and Table 6).

4 | DISCUSSION

4.1 | Key sources of uncertainties in the identified significant trends

The significant historical trends detected by this paper were in agreement with previous studies focusing on observed changes in mean and extreme precipitation across all or parts of the LMRB over time. In particular, these studies likewise reported considerable increases (decreases) in extreme precipitation intensity and frequency indices (Sein *et al.*, 2018), RX1day (Villafuerte and Matsumoto, 2015), annual maximum of 5-day precipitation amounts (Caesar *et al.*, 2011), and wet and dry spells (Sein *et al.*, 2018), across the east, southeast, and northwest of MRB (the west of MRB and the north of LRB) in recent decades. Despite such partial similarities, however, the present study for the first time (based on

TABLE 6 Main results obtained by wavelet transform coherence for the strongest relationships between teleconnections/summer monsoons selected by this study and the first EOF (PC_1) mode of the annual extreme precipitation indices over the LMRB during the water years 1952–2015

		Scale							
		Inter-annual				Decadal			
Annual extreme precipitation index (unit)	**Most influential *teleconnection* or *summer monsoon***	**Duration (phase)**	**Period**	**Phase difference (°)**	**Leads/lags (months)**	**Duration (phase)**	**Period**	**Phase difference (°)**	**Leads/lags (months)**
R95p (mm)	*EASMI*	1–2 years (−)	1969–1970	180	0				
		1–4 years (−)	1974–1986	−90 to −135	/1.5–6 to 3–12				
R99p (mm)	*NAO*	4–6 years (+)	1959–1963	−10	/1–2				
		2–3 years (−)	1978–1980	135	3–5/				
		4–8 years (−)	1978–2000	−150	/4–8				
		1–2 years (−)	2009–2011	170	0–1/				
RX1day (mm)	*NAO*	4–6 years (−)	1959–1961	100	11–16/				
		3–5 years (+)	1995–2005	10	1–2/				
R1mm (days)	*EP/NP*	1–2 year (−)	1954–1964	135	1–3/				
		3–4 year (−)	1978–1983	90–100	8–11 to 9–12/				
		6–8 years (−)	1984–1996	170	2–3/				
		3–4 years (−)	2004–2009	−150	/3–4				
R10mm (days)	*EASMI*	4–6 years (+)	1959–1963	0	0				
		5–6 years (+)	1965–1979	−10	/1–2				
		3–6 years (+)	1980–1985	0	0				
		1–2 years (+)	1995–1997	−30	/1–2				
		1–7 years (+)	2003–2012	0	0				
R20mm (days)	*EASMI*	6–8 years (−)	1959–1970	−170	/2–3				
		1–5 years (−)	1975–1988	−90 to −135	/1–8 to 3–15				
		1–3 year (+)	1994–1998	−30	/1–3				
		1–2 years (−)	2009–2011	−180	0				
CWD (days)	*SOI*					8–15 years (+)	1968–2002	0	0
CDD (days)	*AMO*	3–4 years (+)	1986–1999	45	4–6/				

Note: Teleconnection or summer monsoon leads/lags the EOF (PC_1) mode. The numbers before / means leads, and the numbers after / means lags. (+) In-phase, (−) Anti-phase.

our best knowledge) provides a complementary spatial distribution of variability and trends in historical (1952–2015) extreme precipitation events throughout the LMRB. In what follows, the key sources of uncertainties (in terms of using gridded datasets and defining wet days) in this comprehensive trend analysis are discussed.

4.1.1 | Gauge-based gridded daily precipitation dataset: APHRODITE

Using interpolation methods to create gauge-based gridded products potentially affects extreme precipitation values. This is principally related to the unevenly spatial distribution of observational stations applied for computing precipitation time series in each grid (Haylock *et al*., 2008; Chen *et al*., 2010). Wibig *et al*. (2014) concluded that utilizing more stations for calculating average precipitation data in one grid often increases the total amounts of moderate precipitation, but decreases both the highest daily precipitation amounts and the number of dry days. For generating the APHRODITE data in Southeast Asia employed by the present study, Yatagai *et al*. (2009) reluctantly regridded the raw spatial resolution (0.05° × 0.05°) to 0.25° × 0.25° (Ono *et al*., 2013) due to the data policy of not allowing to release the original time series (Yatagai *et al*., 2012). As a result, therefore, one grid of APHRODITE in Southeast Asia provides spatially averaged precipitation value from 25 raw grids. Such an average is reasonable as a representative daily precipitation value in the 0.25° grid, but generally less than the precipitation records at rain gauges (Ono *et al*., 2013). The regridding process would also lead to more optimistic rather than more pessimistic estimations (Ono *et al*., 2013) of daily precipitation amounts, particularly more than 150 mm. Using the APHRODITE data, hence, can mainly underestimate high-intensity extreme precipitation events in the tropical environment of Southeast Asia, where experiences daily precipitation heavier than 150 mm.

Ono *et al*. (2013) reported that the annual maximum daily precipitation of a 5-year return period for the APHRODITE data in three countries (Laos, Thailand, and Vietnam) of the Greater Mekong Region was approximately 33–38% less than that of the in-situ records. Based on the definition of extreme precipitation events applied by Ono *et al*. (2013), such bias was mostly associated with the daily precipitation events more than 150 mm recorded at 150, 30, and 5 rain gauges in Thailand, Laos, and Vietnam, respectively, during 1987–2006. However, the annual and monthly precipitation of the APHRODITE data in Thailand was about 10–20% less than that of the in-situ records, predominantly due to the underestimation of daily precipitation events more than 150 mm (Ono *et al*., 2013). Thus, the APHRODITE data can practically be employed for identifying all historical extreme precipitation indices in the LMRB, except the maximum 1-day precipitation (RX1day) that might be heavier than 150 mm in some parts of the basin. Accordingly, care should be taken when interpreting the long-term (1952–2015) variability and changes in RX1day (ID No. 3 in Table 1) throughout the LMRB determined based on the APHRODITE data.

4.1.2 | Interchange between wet and dry days

Changes in the frequency of both wet and dry days can cause substantial uncertainties in estimating wet (CWD) and dry (CDD) spells (ID Nos. 7 and 8 in Table 1). It was concluded by Zolina *et al*. (2010), for example, that more frequent wet days can play a crucial role in both shortening and lengthening of wet spell duration. Thus, Zolina *et al*. (2013) proposed a fractional truncated geometric distribution (FTGD) based on the relative contribution of dry and wet spells during a specific period to the total number of dry and wet days. Accordingly, they found lengthening of wet spells during cold months (October–March) throughout the northern parts of Europe, but shortening trends in both dry and wet spells during warm months (April–September). Applying both historical histogram and FTGD approaches, Irannezhad *et* al. (2017) also reported shorter (longer) 1–5 days dry (wet) periods throughout Finland during 1961–2011 in response to less dry (more wet) days.

The present study determined longer (shorter) 1–3 days wet (dry) periods over the LMRB during the water years over 1952–2015 based on the empirical histogram, while shorter wet and longer dry periods (≥1 day) based on the FTGD approach (Figure 10a). Similar results were also found in prolonged (90th percentiles) wet and dry periods mainly across the south and east of LMRB (Figure 10b). Besides, lengthening (shortening) of the longest wet (dry) periods was identified across most parts of LMRB (Figure 10c). Likewise, Zolina *et al*. (2013) and Irannezhad *et* al. (2017) showed that decreases in extremely long dry periods across Scandinavia and Finland, respectively, in recent decades were related to longer prolonged wet periods. Hence, alterations in wet (CWD) and dry (CDD) spells (ID Nos. 7 and 8 in Table 1) are principally not independent, referring to the shorter (longer) CWD in response to longer (shorter) CDD throughout the LMRB.

4.2 | The roles of teleconnections and summer monsoons

Due to climate warming, higher rates of both ocean evaporation and terrestrial evapotranspiration are exacerbating

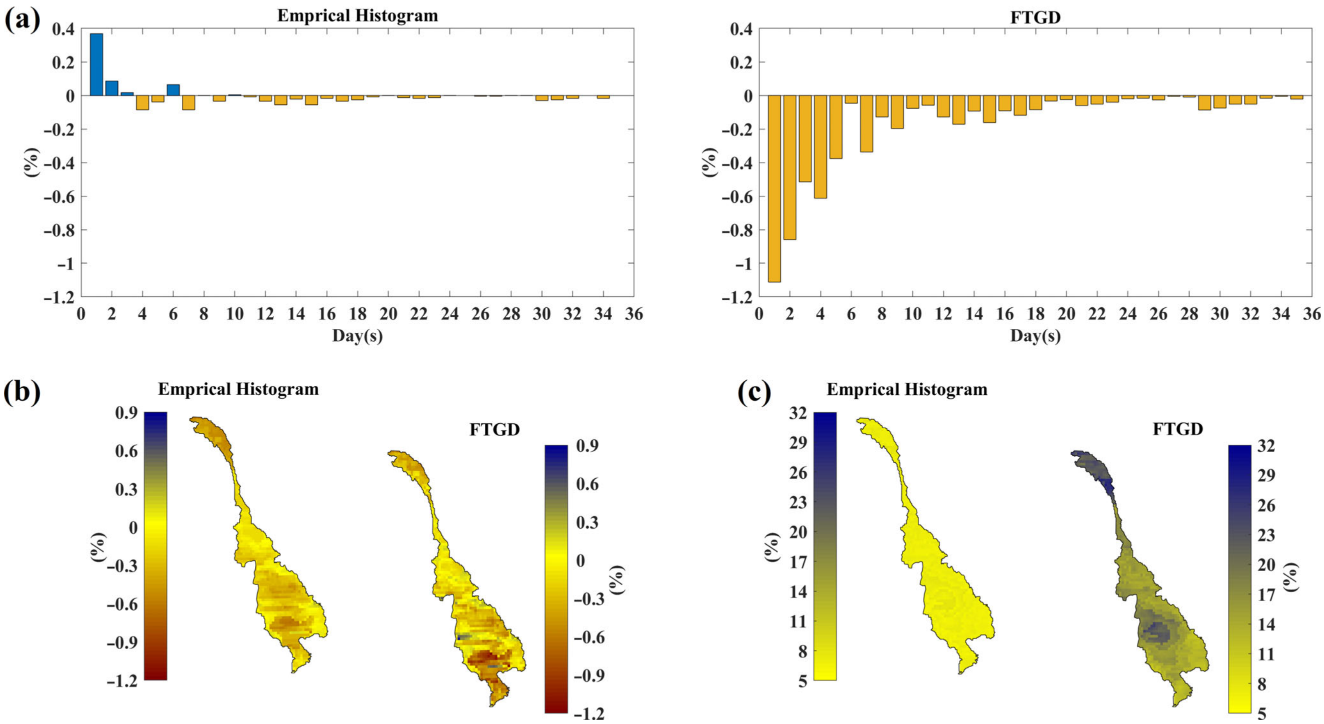

FIGURE 10 Differences in probabilities (%) of (a) various wet and dry periods (1–35 days) on basin-scale of LMRB, (b) prolonged (90th percentiles), and (c) longest wet and dry periods over different parts of the LMRB, estimated by the empirical histogram (left) and FTGD (right) [Colour figure can be viewed at wileyonlinelibrary.com]

the regional water cycle (e.g., IPCC, 2013). Accordingly, the local moisture recycling process leads to more precipitation (Zhang *et al.*, 2017b; Zhang *et al.*, 2017a). The sources and transport pathways of atmospheric moisture (or AWV) are generally driven by different teleconnections and summer monsoons (e.g., Trenberth *et al.*, 2003; Liu *et al.*, 2020), with lagging, concurrent, or leading influences on mean and extreme precipitation characteristics (e.g., Tabari and Willems, 2018; Irannezhad *et al.*, 2020).

Previous studies reported considerable increases in precipitation variability across the LMRB (e.g., Räsänen *et al.*, 2012; Delgado *et al.*, 2012; Lutz *et al.*, 2014). For explaining and interpreting the complex role of teleconnections and/or summer monsoons, the present study first applied the EOF method to decrease the dimensionality of time series for annual extreme precipitation indices across the LMRB. In summary, the first EOF (EOF_1) could represent the most dominant pattern of historical extreme precipitation events throughout the LMRB. Accordingly, the strongest teleconnections or summer monsoons influencing annual extreme precipitation indices over the LMRB during the water years 1952–2015 were identified: the EASMI, NAO, EP/NP, SOI, and AMO. However, confidence in the statistical and physical consistencies for each of these teleconnections or summer monsoon indices with spatio-temporal variability in extreme precipitation characteristics over the LMRB needs to be thoroughly discussed.

- The EASMI—EASMI has most significantly influenced the R95, R10mm, and R20mm across the LMRB in recent decades. Similarly, it was positively in relationship with the R1mm. This summer monsoon (EASMI) is defined as the difference between the westerly anomalies averaged across (5°–15°N, 100°–130°E) and (20°–30°N, 110°–140°E). The EASMI principally regulates the wet season (June–October) precipitation across the southeast of MRB (Xue *et al.*, 2011; Delgado *et al.*, 2012; Tsai *et al.*, 2015). This region was identified by this study as one of the strong centres receiving extreme precipitation events throughout the LMRB. The relatively strong EASMI is originated from the positive diabatic heating anomalies across the northwestern Philippine Islands (Yang *et al.*, 2019). When it is simultaneously associated with the strong ISMI due to the positive diabatic heating anomalies over northeastern India, two anomalous cyclones are developed in the north of the Bay of Bengal (BoB) and the north of the South China Sea (SCS), inducing westerly and easterly anomalies across the northern BoB and the northern SCS, respectively. Accordingly, the anomalous zonal winds carry more atmospheric water vapour from the BoB and the SCS to the LMRB. The unusual convergence zone accompanying such anomalous zonal winds is positioned exactly in the MRB, causing much heavier precipitation events than normal principally over the southern and southeastern parts. The opposite conditions leading to below-normal precipitation in the wet season over the MRB are principally referred to as the relatively weak EASMI and ISM (Yang *et al*., 2019).

- The NAO—the EOF_1s of both R99p and RX1day, as two extreme precipitation intensity indices, over the LMRB showed the strongest coherences with the NAO; particularly over the northern part of LRB located in the Tibetan Plateau (TP). Liu *et al.* (2015b) concluded that the NAO greatly controlled the Dipole Oscillations in the TP summer season (June–August) precipitation by influencing the atmospheric circulation around and across the TP. The regression pattern analysis of the upper-level geopotential heights and the Eliassen-Palm (EP) stationary wave flux with the NAO showed that the stationary wave activity spreading eastward from the North Atlantic pronounces a wave train pattern, which bridges the North Atlantic and the TP during summertime (Jun-Aug) covered by the wet season in the present study (Liu *et al*., 2015b). Accordingly, warm-wet air from the oceans around Asia flows to the northeast of TP during the positive phase of NAO by the southeastern flank of the anticyclonic anomaly across East Asia. The convergence of such warm-wet air mass and the cold airflows transported by the northwestern flank of the cyclonic anomaly braces cumulus convective activities and ultimately causes excessive precipitation over the northeast of TP. Meanwhile, a cyclonic anomaly induces water vapour to condense into precipitation over northwestern India and Pakistan, and thus, inhibits Arabian Sea moisture inflows into the northeast of India and the southeast of TP. Consequently, a precipitation deficit occurs across the north of LRB located in the Southeastern TP. The opposite scenario is accompanied by the negative NAO phase (Liu *et al*., 2015b).
- The EP/NP—the number of wet days (R1mm) showed the strongest correlations with the EP/NP at all three of LRB, MRB, and LMRB during the water years 1952–2015. In general, the negative phase of EP/NP is associated with the positive anomalies of SST in the SCS forcing both low-level convergence and convection intensification that together substantially increases precipitation in Central Vietnam (covering the east of MRB) and the Philippines during the autumn (October–December) season (Li *et al*., 2015).
- The SOI—SOI is most significantly associated with the CWD over the LMRB in recent decades. During the negative/positive SOI (El Niño/La Niña) events, the Walker circulation and the trade winds are simultaneously weakened/strengthened in response to decreases/increases in the southeast to southwest Pacific Ocean temperature difference. With the lower/higher ocean temperatures, Southeast Asia (partially covering the LMRB) experiences less/more evaporation and clouds, and consequently less/ more precipitation (Cherchi and Navarra, 2013; Räsänen and Kummu, 2013; Räsänen *et al*., 2016; Hrudya *et al*., 2020; Irannezhad *et al*., 2020). During El Niño/La Niña events, the temperatures over the BoB, Indian Ocean, and the Arabian Sea also persist above/below normal. Therefore, the low (high) pressure difference between these water bodies to the south and the Asian mainland to the north significantly moderates (intensifies) the AWV flow to the LMRB, causing less (more) precipitation over this basin (e.g., Cherchi and Navarra, 2013; Hrudya *et al*., 2020).
- The AMO—AMO was the strongest teleconnection influencing the CDD in the LMRB on the interannual time scale of 3–4 years through 1986–1999, with the leading time of 4–6 months. This teleconnection (AMO) is a quasi-periodic warm and cold anomaly happening in the sea surface temperature of the North Atlantic, at the sea basin scale in space and multi-decadal scale in time (Enfield *et al*., 2001; Teegavarapu *et al*., 2013; Veres and Hu, 2013). Although the AMO plays a key role in climate variability across North America and Europe (Veres and Hu, 2013; Goly and Teegavarapu, 2014), Qian *et al.* (2014) and Ding *et al.* (2019) reported its higher positive influence than the Asian summer monsoons (ISMI, EASMI, SASMI, and SCSMI) on the extreme precipitation indices, particularly CDD, over the north of LRB. Similarly, other previous studies also concluded that the positive phase of AMO naturally increases precipitation over the West Pacific, covering the LMRB (Verdon and Franks, 2006; Delgado *et al*., 2012;Chen *et al*., 2019). In general, the AMO lags (leads) the PDO by 17 (13) years during the same 60-year oscillation cycle (d'Orgeville and Peltier, 2007). Hence, the positive AMO phase is simultaneously associated with the negative phase of PDO, which considerably increases precipitation in the west pacific, covering the LMRB, by warming sea surface temperature and consequently intensifying the rate of ocean evaporation over the same region.

Landfalling TCs can transport abundant AWV contents resulting in extreme precipitation events (Smith *et al*., 2011). Such TCs are strongly associated with large-scale oceanic-atmospheric teleconnections, for example, PDO or SOI (Walsh *et al*., 2016). TCs influencing the LMRB are formed in the South China Sea (SCS), North Indian Ocean (NIO) or BoB, and western North Pacific

Ocean (WNP) (Chen *et al*., 2019). Previous studies reported fewer TCs from the WNP to the SCS during the positive PDO phase (Goh and Chan, 2010; Lee *et al*., 2012), which is in line with the negative phase of SOI or El Niño (Verdon and Franks, 2006; Delgado *et al*., 2012). The NIO or BoB TCs also show less activity under the positive PDO and negative SOI phases (Ng and Chan, 2012), while the response of TCs formed in the SCS is not clear (Goh and Chan, 2010). Chen *et al*. (2019), however, concluded no significant correlations between these two teleconnections (PDO and SOI) and the TCs associated precipitation over the LMRB during 1983–2016.

5 | CONCLUSIONS

The present study determined the climatology and trends of annual extreme precipitation indices throughout the LMRB during the water years 1952–2015. The interannual variations in these indices were related to seven teleconnection and summer monsoon indices. The major conclusions were:

- On the basin scale, no significant historical trends were detected in annual extreme precipitation indices across the LMRB. The number of wet days (R1mm) significantly ($p < .05$) increased in both MRB and the LRB during the water years 1952–2015; essentially leading to longer wet spells (CWD) in these two subbasins. However, an increasing trend in the R1mm across the LMRB during the same study period was statistically insignificant.
- Spatially, annual extreme precipitation indices (R95p, R99p, and RX1day) increased across the south, southeast, and northwest of MRB over time, while decreased throughout the west of MRB and most parts of the LRB. The number of wet (R1mm), heavy (R10mm), and very heavy (R20mm) precipitation events also increased over the southeast and north of MRB, while decreased in the west of MRB. Accordingly, lengthening (shortening) trends in wet spells were identified in the east and northwest of MRB (some areas in the west MRB), while longer (shorter) dry spells were found over some areas in the east of MRB as well as the south of LRB (several grids in the east and west of MRB).
- The three leading patterns (EOF_{1-3}) of annual extreme precipitation indices revealed that historical variations in extreme precipitation events were more complex to identify across the MRB than over the LRB. As the most dominant pattern, however, the EOF_1s were highly consistent with the spatial distribution of typical variations in annual extreme precipitation indices throughout the LMRB during the water years 1952–2015.
- In general, the year-to-year variations in both the intensity and frequency of historical extreme precipitation events in the LMRB were most significantly associated with the EASMI, NAO, and EP/NP. As one of the annual extreme precipitation duration indices, wet spells (CWD) had the strongest relationship with the AMO on the interannual time scale of 3–4 years during 1986–1999, with a phase difference of 45°, indicating that the AMO leads the CWD by 4–6 months. As the other annual extreme precipitation duration index, however, the CDD showed the most significant coherences with the SOI on the decadal time scale of 8–15 years during 1968–2002, with a phase difference of 0° (simultaneous).

ACKNOWLEDGEMENTS

The Strategic Priority Research Program of the Chinese Academy of Sciences funded this study by grant number XDA20060401. The National Natural Science Foundation of China with grant number 41625001, the High-level Special Funding of the Southern University of Science and Technology with the grant numbers G02296302 and G02296402 are also acknowledged for partially financing this study. J.L. would like to thank: the Pengcheng Scholar Program of Shenzhen, the National High-level Talents Special Support Plan ("Ten Recruitment Program of Global Experts"), the Leading Innovative Talent Program for young and middle-aged scholars by the Ministry of Science and Technology, and the Swedish STINT (CH2019-8377).

AUTHOR CONTRIBUTIONS

Masoud Irannezhad: Conceptualization; formal analysis; investigation; methodology; software; validation; visualization; writing – original draft; writing – review and editing. **Deliang Chen:** Funding acquisition; project administration; resources; supervision; writing – review and editing.

ORCID

Junguo Liu https://orcid.org/0000-0002-5745-6311
Deliang Chen https://orcid.org/0000-0003-0288-5618

REFERENCES

Alexander, L.V., Zhang, X., Peterson, T.C., Caesar, J., Gleason, B., Klein Tank, A.M.G., Haylock, M., Collins, D., Trewin, B., Rahimzadeh, F., Tagipour, A., Rupa Kumar, K., Revadekar, J., Griffiths, G., Vincent, L., Stephenson, D.B., Burn, J., Aguilar, E., Brunet, M., Taylor, M., New, M., Zhai, P., Rusticucci, M. and Vazquez-Aguirre, J.L. (2006) Global observed changes in daily climate extremes of temperature and precipitation. *Journal of Geophysical Research Atmospheres*, 111 (D5), D05109. https://doi.org/10.1029/2005JD006290.

Ali, H. and Mishra, V. (2017) Contrasting response of rainfall extremes to increase in surface air and dewpoint temperatures at urban locations in India. *Scientific Reports*, 7(1), 1228. https://doi.org/10.1038/s41598-017-01306-1.

Asong, Z.E., Wheater, H.S., Bonsal, B., Razavi, S. and Kurkute, S. (2018) Historical drought patterns over Canada and their teleconnections with large-scale climate signals. *Hydrology and Earth System Sciences*, 22, 3105–3124. https://doi.org/10.5194/hess-22-3105-2018.

Bagtasa, G. (2020) 118-year climate and extreme weather events of metropolitan Manila in The Philippines. *International Journal of Climatology*, 40, 1228–1240. https://doi.org/10.1002/joc.6267.

Bâki Iz, H.B. (2018) Is the global sea surface temperature rise accelerating? *Geodesy and Geodynamics*, 9(6), 432–438. https://doi.org/10.1016/j.geog.2018.04.002.

Barnston, A.G. and Livezey, R.E. (1987) Classification, seasonality and persistence of low-frequency atmospheric circulation patterns. *Monthly Weather Review*, 115, 1083–1126. https://doi.org/10.1175/1520-0493(1987)115<1083:CSAPOL>2.0.CO;2.

Barros, V.R., Field, C.B., Dokken, D.J., Mastrandrea, M.D., Mach, K.J., Bilir, T.E., Chatterjee, M., Ebi, K.L., Estrada, Y.O., Genova, R.C., Girma, B., Kissel, E.S., Levy, A.N., MacCracken, S., Mastrandrea, P.R., and White, L.L. (2014). *Climate change 2014 impacts, adaptation, and vulnerability Part B: Regional aspects: Working group ii contribution to the fifth assessment report of the intergovernmental panel on climate change*. *Climate Change 2014: Impacts, Adaptation and Vulnerability: Part B: Regional Aspects: Working Group II Contribution to the Fifth Assessment Report of the Intergovernmental Panel on Climate Change*.

Bayazit, M. and Önöz, B. (2007) To prewhiten or not to prewhiten in trend analysis? *Hydrological Science Journal*, 52(4), 611–624.

Bengtsson, L. (2010) The global atmospheric water cycle. *Environmental Research Letters*, 5(2), 025202.

Caesar, J., Alexander, L.V., Trewin, B., Tse-ring, K., Sorany, L., Vuniyayawa, V., Keosavang, N., Shimana, A., Htay, M.M., Karmacharya, J., Jayasinghearachchi, D.A., Sakkamart, J., Soares, E., Hung, L.T., Thuong, L.T., Hue, C.T., Dung, N.T.T., Hung, P.V., Cuong, H.D., Cuong, N.M. and Sirabaha, S. (2011) Changes in temperature and precipitation extremes over the Indo-Pacific region from 1971 to 2005. *International Journal of Climatology*, 31, 791–801. https://doi.org/10.1002/joc.2118.

Chang, C.P., Wang, Z., McBride, J. and Liu, C.H. (2005) Annual cycle of Southeast Asia—maritime continent rainfall and the asymmetric monsoon transition. *Journal of Climate*, 18, 287–301. https://doi.org/10.1175/JCLI-3257.1.

Chen, A., Chen, D. and Azorin-Molina, C. (2018) Assessing reliability of precipitation data over the Mekong River basin: a comparison of ground-based, satellite, and reanalysis datasets. *International Journal of Climatology*. 38(11), 4314–4334. https://doi.org/10.1002/joc.5670.

Chen, A., Ho, C.H., Chen, D. and Azorin-Molina, C. (2019) Tropical cyclone rainfall in the Mekong River Basin for 1983–2016. *Atmospheric Research*, 226, 66–75. https://doi.org/10.1016/j.atmosres.2019.04.012.

Chen, D., Ou, T., Gong, L., Xu, C.Y., Li, W., Ho, C.H. and Qian, W. (2010) Spatial interpolation of daily precipitation in China: 1951-2005. *Advances in Atmospheric Sciences*, 27, 1221–1232. https://doi.org/10.1007/s00376-010-9151-y.

Cherchi, A. and Navarra, A. (2013) Influence of ENSO and of the Indian Ocean dipole on the Indian summer monsoon variability. *Climate Dynamics*, 41, 81–103. https://doi.org/10.1007/s00382-012-1602-y.

Choi, J.H., Yoon, T.H., Kim, J.S. and Moon, Y.I.L. (2018) Dam rehabilitation assessment using the Delphi-AHP method for adapting to climate change. *Journal of Water Resources Planning and Management*, 144, 6017007. https://doi.org/10.1061/(ASCE)WR.1943-5452.0000877.

Collins, M., R. Knutti, J. Arblaster, J.-L. Dufresne, T. Fichefet, P. Friedlingstein, X. Gao, W.J. Gutowski, T. Johns, G. Krinner, M. Shongwe, C. Tebaldi, A.J. Weaver and M. Wehner, 2013: Long-term Climate Change: Projections, Commitments and Irreversibility. In: *Climate Change 2013: The Physical Science Basis. Contribution of Working Group I to the Fifth Assessment Report of the Intergovernmental Panel on Climate Change* [Stocker, T. F., D. Qin, G.-K. Plattner, M. Tignor, S.K. Allen, J. Boschung, A. Nauels, Y. Xia, V. Bex and P.M. Midgley (eds.)]. Cambridge University Press, Cambridge, United Kingdom and New York, NY, USA.

Delgado, J.M., Merz, B. and Apel, H. (2012) A climate-flood link for the lower Mekong River. *Hydrology and Earth System Sciences*, 16, 1533–1541. https://doi.org/10.5194/hess-16-1533-2012.

Ding, Z., Lu, R. and Wang, Y. (2019) Spatiotemporal variations in extreme precipitation and their potential driving factors in non-monsoon regions of China during 1961-2017. *Environmental Research Letters*, 14(2), 024005. https://doi.org/10.1088/1748-9326/aaf2ec.

Donat, M.G., Lowry, A.L., Alexander, L.V., O'Gorman, P.A. and Maher, N. (2016) More extreme precipitation in the world's dry and wet regions. *Nature Climate Change*, 6, 508–513. https://doi.org/10.1038/nclimate2941.

Dong, X., Zhang, S., Zhou, J., Cao, J., Jiao, L., Zhang, Z. and Liu, Y. (2019) Magnitude and frequency of temperature and precipitation extremes and the associated atmospheric circulation patterns in the Yellow River Basin (1960–2017), China. *Water*, 11 (11), 2334. https://doi.org/10.3390/w11112334.

d'Orgeville, M. and Peltier, W.R. (2007) On the Pacific Decadal Oscillation and the Atlantic Multidecadal Oscillation: might they be related? *Geophysical Research Letters*, 34(23), L23705. https://doi.org/10.1029/2007GL031584.

Dugan, P.J., Barlow, C., Agostinho, A.A., Baran, E., Cada, G.F., Chen, D., Cowx, I.G., Ferguson, J.W., Jutagate, T., Mallen-Cooper, M., Marmulla, G., Nestler, J., Petrere, M., Welcomme, R.L. and Winemiller, K.O. (2010) Fish migration, dams, and loss of ecosystem services in the mekong basin. *Ambio*, 39, 344–348. https://doi.org/10.1007/s13280-010-0036-1.

Enfield, D.B., Mestas-Nuñez, A.M. and Trimble, P.J. (2001) The Atlantic multidecadal oscillation and its relation to rainfall and river flows in the continental U.S. *Geophysical Research Letters*, 28, 2077–2080. https://doi.org/10.1029/2000GL012745.

Fan, X. and Luo, X. (2019) Precipitation and flow variations in the Lancang-Mekong River Basin and the implications of monsoon fluctuation and regional topography. *Water (Switzerland)*, 11 (10), 2086. https://doi.org/10.3390/w11102086.

Fang, K., Chen, D., Ilvonen, L., Pasanen, L., Holmström, L., Seppä, H., Huang, G., Ou, T. and Linderholm, H. (2019)

Oceanic and atmospheric modes in the Pacific and Atlantic oceans since the little ice age (LIA): towards a synthesis. *Quaternary Science Reviews*. 215, 293–307. https://doi.org/10.1016/j.quascirev.2019.05.014.

Goh, A.Z.C. and Chan, J.C.L. (2010) Interannual and interdecadal variations of tropical cyclone activity in the South China Sea. *International Journal of Climatology*, 30, 827–843. https://doi.org/10.1002/joc.1943.

Goly, A. and Teegavarapu, R.S.V. (2014) Individual and coupled influences of AMO and ENSO on regional precipitation characteristics and extremes. *Water Resources Research*, 50, 4686–4709. https://doi.org/10.1002/2013WR014540.

Grinsted, A., Moore, J.C. and Jevrejeva, S. (2004) Application of the cross wavelet transform and wavelet coherence to geophysical time series. *Nonlinear Processes in Geophysics*, 11, 561–566. https://doi.org/10.5194/npg-11-561-2004.

Gupta, A. (2007) The Mekong River: morphology, evolution, management. In: Gupta, A. (Ed.) *Large Rivers: Geomorphology and Management*. Chichester: John Wiley, pp. 435–455.

Hannachi, A., Jolliffe, I.T. and Stephenson, D.B. (2007) Empirical orthogonal functions and related techniques in atmospheric science: a review. *International Journal of Climatology*, 27, 1119–1152.

Haylock, M.R., Hofstra, N., Klein Tank, A.M.G., Klok, E.J., Jones, P. D. and New, M. (2008) A European daily high-resolution gridded data set of surface temperature and precipitation for 1950-2006. *Journal of Geophysical Research Atmospheres*, 113(D20), D20119. https://doi.org/10.1029/2008JD010201.

Helsel, D.R. and Hirsch, R.M. (1992) Statistical methods in water resources. *Technometrics*, 36, 323. https://doi.org/10.2307/1269385.

Hrudya, P.H., Varikoden, H. and Vishnu, R. (2020) A review on the Indian summer monsoon rainfall, variability and its association with ENSO and IOD. *Meteorology and Atmospheric Physics*, 133, 1–14. https://doi.org/10.1007/s00703-020-00734-5.

IPCC Working Group 1 I, Stocker, T.F., Qin, D., Plattner, G.-K., Tignor, M., Allen, S.K., Boschung, J., Nauels, A., Xia, Y., Bex, V., and Midgley, P.M. (2013). *IPCC, 2013: Climate Change 2013: The Physical Science Basis*. Contribution of Working Group I to the Fifth Assessment Report of the Intergovernmental Panel on Climate Change. IPCC.

Irannezhad, M., Chen, D., Kløve, B. and Moradkhani, H. (2017) Analysing the variability and trends of precipitation extremes in Finland and their connection to atmospheric circulation patterns. *International Journal of Climatology*, 37, 1053–1066. https://doi.org/10.1002/joc.5059.

Irannezhad, M., Liu, J. and Chen, D. (2020) Influential climate teleconnections for spatiotemporal precipitation variability in the Lancang-Mekong River Basin from 1952 to 2015. *Journal of Geophysical Research: Atmospheres*, 125(21), e2020JD033331. https://doi.org/10.1029/2020jd033331.

Irannezhad, M., Marttila, H., Chen, D. and Kløve, B. (2016) Century-long variability and trends in daily precipitation characteristics at three Finnish stations. *Advances in Climate Change Research*, 7, 54–69. https://doi.org/10.1016/j.accre.2016.04.004.

Jiang, R., Wang, Y., Xie, J., Zhao, Y., Li, F. and Wang, X. (2019) Assessment of extreme precipitation events and their teleconnections to El Niño Southern Oscillation, a case study in the Wei River Basin of China. *Atmospheric Research*, 218, 372–384. https://doi.org/10.1016/j.atmosres.2018.12.015.

Jiang, Z., Shuai, J., Yi, S., Liu, Z., Wei, L. and Li, L. (2017) Impact of moisture source variation on decadal-scale changes of precipitation in North China from 1951 to 2010: moisture source variation. *Journal of Geophysical Research*, 122, 600–613.

Kendall, M.G. (1975) Rank correlation methods. *Biometrika*, 44, 298. https://doi.org/10.2307/2333282.

Kirchmeier-Young, M. and Zhang, X. (2020) Human influence has intensified extreme precipitation in North America. *PNAS*, 177(24), 13308–13313. https://doi.org/10.1073/pnas.1921628117.

Kirtman, B., S.B. Power, J.A. Adedoyin, G.J. Boer, R. Bojariu, I. Camilloni, F.J. Doblas-Reyes, A.M. Fiore, M. Kimoto, G.A. Meehl, M. Prather, A. Sarr, C. Schär, R. Sutton, G.J. van Oldenborgh, G. Vecchi and H.J. Wang, 2013: Near-term Climate Change: Projections and Predictability. In: *Climate Change 2013: The Physical Science Basis. Contribution of Working Group I to the Fifth Assessment Report of the Intergovernmental Panel on Climate Change* [Stocker, T.F., D. Qin, G.-K. Plattner, M. Tignor, S.K. Allen, J. Boschung, A. Nauels, Y. Xia, V. Bex and P.M. Midgley (eds.)]. Cambridge University Press, Cambridge, United Kingdom and New York, NY, USA.

Leander, R., Buishand, T.A. and Klein Tank, A.M.G. (2014) An alternative index for the contribution of precipitation on very wet days to the total precipitation. *Journal of Climate*, 27, 1365–1378. https://doi.org/10.1175/JCLI-D-13-00144.1.

Lee, T., Leung, C.Y., Kok, M. and Chan, H. (2012) The long term variations of tropical cyclone activity in the South China Sea and the vicinity of Hong Kong. *Tropical Cyclone Research and Review*. 1(3), 277–292. https://doi.org/10.6057/2012TCRR02.01.

Li, J. and Zeng, Q. (2002) A unified monsoon index. *Geophysical Research Letters*, 29, 115-1–115-4. https://doi.org/10.1029/2001GL013874.

Li, J. and Zeng, Q. (2003) A new monsoon index and the geographical distribution of the global monsoons. *Advances in Atmospheric Sciences*, 20, 299–302. https://doi.org/10.1007/s00376-003-0016-5

Li, R., Wang, S.Y., Gillies, R.R., Buckley, B.M., Truong, L.H. and Cho, C. (2015) Decadal oscillation of autumn precipitation in Central Vietnam modulated by the East Pacific-North Pacific (EP-NP) teleconnection. *Environmental Research Letters*, 10(2), 024008. https://doi.org/10.1088/1748-9326/10/2/024008.

Lin, L., Xu, Y., Wang, Z., Diao, C., Dong, W. and Xie, S.P. (2018) Changes in extreme rainfall over India and China attributed to regional aerosol-cloud interaction during the late 20th century rapid industrialization. *Geophysical Research Letters*, 45, 7857–7865. https://doi.org/10.1029/2018GL078308.

Liu, A., Soneja, S.I., Jiang, C., Huang, C., Kerns, T., Beck, K., Mitchell, C. and Sapkota, A. (2017) Frequency of extreme weather events and increased risk of motor vehicle collision in Maryland. *Science of the Total Environment*, 580, 550–555. https://doi.org/10.1016/j.scitotenv.2016.11.211.

Liu, B., Tan, X., Gan, T.Y., Chen, X., Lin, K., Lu, M. and Liu, Z. (2020) Global atmospheric moisture transport associated with precipitation extremes: mechanisms and climate change impacts. *WIREs Water*, 7(2), e1412. https://doi.org/10.1002/wat2.1412.

Liu, H., Duan, K., Li, M., Shi, P., Yang, J., Zhang, X. and Sun, J. (2015b) Impact of the North Atlantic oscillation on the dipole oscillation of summer precipitation over the central and eastern

Tibetan plateau. *International Journal of Climatology*, 35, 4539–4546. https://doi.org/10.1002/joc.4304.

Liu, R., Liu, S.C., Cicerone, R.J., Shiu, C.J., Li, J., Wang, J. and Zhang, Y. (2015a) Trends of extreme precipitation in eastern China and their possible causes. *Advances in Atmospheric Sciences*, 32, 1027–1037. https://doi.org/10.1007/s00376-015-5002-1.

Liu, Y., Zhang, C., Tang, Q., Hosseini-Moghari, S.-M., Haile, G.C., Li, L., Li, W., Yang, K., van der Ent, R.J. and Chen, D. (2021) Moisture source variations for summer rainfall in different intensity classes over Huaihe River valley, China. *Climate Dynamics*, 57, 1121–1133. https://doi.org/10.1007/s00382-021-05762-4.

Lorenz, E.N. (1956). Empirical orthogonal functions and statistical weather prediction. *Technical report Statistical Forecast Project Report 1 Department of Meteorology MIT 49*.

Lutz, A., Terink, W., Droogers, P., Immerzeel, W., and Piman, T. (2014). Development of baseline climate data set and trend analysis in the Mekong Basin. 1–127.

Ma, Q., Zhang, J., Teshome, G., Chang, Y. and Li, S. (2020) Spatio-temporal variability of summer precipitation and precipitation extremes and associated large-scale mechanisms in Central Asia during 1979–2018. *Journal of Hydrology X*, 8, 100061. https://doi.org/10.1016/j.hydroa.2020.100061.

Ma, Y., Lu, M., Chen, H., Pan, M. and Hong, Y. (2018) Atmospheric moisture transport versus precipitation across the Tibetan plateau: a mini-review and current challenges. *Atmospheric Research*, 209, 50–58.

Mann, H.B. (1945) Non-parametric test against trend. *Econometrica*, 13, 245.

Mishra, V., Wallace, J.M. and Lettenmaier, D.P. (2012) Relationship between hourly extreme precipitation and local air temperature in the United States. *Geophysical Research Letters*, 39(16), L16403. https://doi.org/10.1029/2012GL052790.

Misra, V. and Dinapoli, S. (2014) The variability of the southeast Asian summer monsoon. *International Journal of Climatology*, 34, 893–901. https://doi.org/10.1002/joc.3735.

MRC. (2010). *Mekong River Commission: State of the Basin Report 2010*. .

MRC. (2015). *Annual mekong flood report 2013*. Vientiane, Lao PDR.

Mukherjee, S., Aadhar, S., Stone, D. and Mishra, V. (2018) Increase in extreme precipitation events under anthropogenic warming in India. *Weather and Climate Extremes*, 20, 45–53. https://doi.org/10.1016/j.wace.2018.03.005.

Myhre, G., Alterskjær, K., Stjern, C.W., Hodnebrog, Ø., Marelle, L., Samset, B.H., Sillmann, J., Schaller, N., Fischer, E., Schulz, M. and Stohl, A. (2019) Frequency of extreme precipitation increases extensively with event rareness under global warming. *Scientific Reports*, 9, 16063. https://doi.org/10.1038/s41598-019-52277-4.

Ng, E.K.W. and Chan, J.C.L. (2012) Interannual variations of tropical cyclone activity over the North Indian Ocean. *International Journal of Climatology*, 32, 819–830. https://doi.org/10.1002/joc.2304.

North, G.R., Bell, T.L., Cahalan, R.F. and Moeng, F.J. (1982) Sampling errors in the estimation of empirical orthogonal functions. *Monthly Weather Review*, 110, 699–706. https://doi.org/10.1175/1520-0493(1982)110<0699:seiteo>2.0.co;2.

O'Gorman, P.A. and Schneider, T. (2009) The physical basis for increases in precipitation extremes in simulations of 21st-century climate change. *Proceedings of the National Academy of Sciences of the United States of America*, 106, 14773–14777. https://doi.org/10.1073/pnas.0907610106.

Ohba, M. and Sugimoto, S. (2019) Differences in climate change impacts between weather patterns: possible effects on spatial heterogeneous changes in future extreme rainfall. *Climate Dynamics*, 52, 4177–4191. https://doi.org/10.1007/s00382-018-4374-1.

Ono, K., Kazama, S., Gunawardhana, L.N. and Kuraji, K. (2013) An investigation of extreme daily rainfall in the Mekong River Basin using a gridded precipitation dataset. *Hydrological Research Letters*, 7, 66–72. https://doi.org/10.3178/hrl.7.66.

Papalexiou, S.M. and Montanari, A. (2019) Global and regional increase of precipitation extremes under global warming. *Water Resources Research*, 55, 4901–4914. https://doi.org/10.1029/2018WR024067.

Park, E. and Lee, Y.J. (2001) Estimates of standard deviation of Spearman's rank correlation coefficients with dependent observations. *Communications in Statistics Part B: Simulation and Computation*, 30, 129–142. https://doi.org/10.1081/SAC-100001863.

Pathak, A., Ghosh, S., Martinez, J.A., Dominguez, F. and Kumar, P. (2016) Role of oceanic and land moisture sources and transport in the seasonal and inter-annual variability of summer monsoon in India. *Journal of Climate*, 30(15), 1839–1859. https://doi.org/10.1175/JCLI-D-16-0156.1.

Phi Hoang, L., Lauri, H., Kummu, M., Koponen, J., Van Vliet, M.T. H.V.H., Supit, I., Leemans, R., Kabat, P., Ludwig, F., Hoang, L. P., Lauri, H., Kummu, M., Koponen, J., Van Vliet, M.T.H.V.H., Supit, I., Leemans, R., Kabat, P. and Ludwig, F. (2016) Mekong River flow and hydrological extremes under climate change. *Hydrology and Earth System Sciences*, 20(7), 3027–3041. https://doi.org/10.5194/hess-20-3027-2016.

Pokhrel, Y., Burbano, M., Roush, J., Kang, H., Sridhar, V. and Hyndman, D.W. (2018) A review of the integrated effects of changing climate, land use, and dams on Mekong river hydrology. *Water*, 10(3), 266. https://doi.org/10.3390/w10030266.

Qian, C., Yu, J.Y. and Chen, G. (2014) Decadal summer drought frequency in China: the increasing influence of the Atlantic Multi-decadal Oscillation. *Environmental Research Letters*. 9 (12), 124004. https://doi.org/10.1088/1748-9326/9/12/124004.

Qian, Y., Gong, D., Fan, J., Ruby Leung, L., Bennartz, R., Chen, D. and Wang, W. (2009) Heavy pollution suppresses light rain in China: observations and modeling. *Journal of Geophysical Research Atmospheres*. 114(D7), D00K02. https://doi.org/10.1029/2008JD011575.

Ramanathan, V. and Feng, Y. (2009) Air pollution, greenhouse gases and climate change: global and regional perspectives. *Atmospheric Environment*, 43, 37–50. https://doi.org/10.1016/j.atmosenv.2008.09.063.

Rana, A., Moradkhani, H. and Qin, Y. (2017) Understanding the joint behavior of temperature and precipitation for climate change impact studies. *Theoretical and Applied Climatology*, 129, 321–339. https://doi.org/10.1007/s00704-016-1774-1.

Räsänen, T.A., Koponen, J., Lauri, H. and Kummu, M. (2012) Downstream hydrological impacts of hydropower development in the Upper Mekong Basin. *Water Resources Management*, 26(12), 3495–3513. https://doi.org/10.1007/s11269-012-0087-0.

Räsänen, T.A. and Kummu, M. (2013) Spatiotemporal influences of ENSO on precipitation and flood pulse in the Mekong River basin. *Journal of Hydrology*, 476, 154–168. https://doi.org/10.1016/j.jhydrol.2012.10.028.

Räsänen, T.A., Lindgren, V., Guillaume, J.H.A., Buckley, B.M. and Kummu, M. (2016) On the spatial and temporal variability of ENSO precipitation and drought teleconnection in mainland Southeast Asia. *Climate of the Past*, 12, 1889–1905. https://doi.org/10.5194/cp-12-1889-2016.

Sein, K.K., Chidthaisong, A. and Oo, K.L. (2018) Observed trends and changes in temperature and precipitation extreme indices over Myanmar. *Atmosphere*, 9(12). 477. https://doi.org/10.3390/atmos9120477.

Sen, P.K. (1968) Estimates of the regression coefficient based on Kendall's tau. *Journal of the American Statistical Association*, 63, 1379–1389. https://doi.org/10.1080/01621459.1968.10480934.

Sidike, A., Chen, X., Liu, T., Durdiev, K. and Huang, Y. (2016) Investigating alternative climate data sources for hydrological simulations in the upstream of the Amu Darya river. *Water (Switzerland)*, 8(10), 441. https://doi.org/10.3390/w8100441.

Sillmann, J., Kharin, V.V., Zwiers, F.W., Zhang, X. and Bronaugh, D. (2013) Climate extremes indices in the CMIP5 multimodel ensemble: part 2. Future climate projections. *Journal of Geophysical Research Atmospheres*, 118, 2473–2493. https://doi.org/10.1002/jgrd.50188.

Smith, J.A., Villarini, G. and Baeck, M.L. (2011) Mixture distributions and the hydroclimatology of extreme rainfall and flooding in the eastern United States. *Journal of Hydrometeorology*, 12, 294–309. https://doi.org/10.1175/2010JHM1242.1.

Su, L., Miao, C., Duan, Q., Lei, X. and Li, H. (2019) Multiple-wavelet coherence of World's large rivers with meteorological factors and ocean signals. *Journal of Geophysical Research: Atmospheres*. 124 (9), 4932–4954. https://doi.org/10.1029/2018JD029842.

Sun, Q., Miao, C., Duan, Q., Ashouri, H., Sorooshian, S. and Hsu, K.L. (2018) A review of global precipitation data sets: data sources, estimation, and Intercomparisons. *Reviews of Geophysics*. 56(1), 79–107. https://doi.org/10.1002/2017RG000574.

Tabari, H. (2020) Climate change impact on flood and extreme precipitation increases with water availability. *Scientific Reports*, 10, 13768. https://doi.org/10.1038/s41598-020-70816-2.

Tabari, H., Hosseinzadehtalaei, P., AghaKouchak, A. and Willems, P. (2019) Latitudinal heterogeneity and hotspots of uncertainty in projected extreme precipitation. *Environmental Research Letters*, 14, 124032. https://doi.org/10.1088/1748-9326/ab55fd.

Tabari, H., Madani, K. and Willems, P. (2020) The contribution of anthropogenic influence to more anomalous extreme precipitation in Europe. *Environmental Research Letters*, 15, 104077. https://doi.org/10.1088/1748-9326/abb268.

Tabari, H. and Willems, P. (2018) Lagged influence of Atlantic and Pacific climate patterns on European extreme precipitation. *Scientific Reports*, 8, 5748. https://doi.org/10.1038/s41598-018-24069-9.

Tan, M.L., Gassman, P.W. and Cracknell, A.P. (2017) Assessment of three long-term gridded climate products for hydro-climatic simulations in tropical river basins. *Water (Switzerland)*, 9(3), 229. https://doi.org/10.3390/w9030229.

Tanarhte, M., Hadjinicolaou, P. and Lelieveld, J. (2012) Intercomparison of temperature and precipitation data sets based on observations in the Mediterranean and the Middle East. *Journal of Geophysical Research Atmospheres*, 117(D12), D12102. https://doi.org/10.1029/2011JD017293.

Teegavarapu, R.S.V., Goly, A. and Obeysekera, J. (2013) Influences of Atlantic multidecadal oscillation phases on spatial and temporal variability of regional precipitation extremes. *Journal of Hydrology*, 495, 74–93. https://doi.org/10.1016/j.jhydrol.2013.05.003.

Thi, M.M., Gunawardhana, L.N. and Kazama, S. (2012) A comparison of historical land-use change patterns and recommendations for flood plain developments in three delta regions in Southeast Asia. *Water International*, 37, 218–235. https://doi.org/10.1080/02508060.2012.687511.

Thompson, D.W.J. and Wallace, J.M. (1998) The Arctic oscillation signature in the wintertime geopotential height and temperature fields. *Geophysical Research Letters*, 25, 1297–1300. https://doi.org/10.1029/98GL00950.

Torrence, C. and Compo, G.P. (1998) A practical guide to wavelet analysis. *Bulletin of the American Meteorological Society*, 79, 61–78. https://doi.org/10.1175/1520-0477(1998)079<0061:APGTWA>2.0.CO;2.

Trenberth, K.E. (1984) Signal versus noise in the Southern Oscillation. *Monthly Weather Review*, 112, 326–332. https://doi.org/10.1175/1520-0493(1984)112<0326:SVNITS>2.0.CO;2.

Trenberth, K.E., Dai, A., Rasmussen, R.M. and Parsons, D.B. (2003) The changing character of precipitation. *Bulletin of the American Meteorological Society*, 84, 1205–1218.

Tsai, C.L., Behera, S.K. and Waseda, T. (2015) Indo-China monsoon indices. *Scientific Reports*, 5, 8107. https://doi.org/10.1038/srep08107.

Turner, A.G. and Annamalai, H. (2012) Climate change and the South Asian summer monsoon. *Nature Climate Change*, 2, 587–595. https://doi.org/10.1038/nclimate1495

Ul Hasson, S., Pascale, S., Lucarini, V. and Böhner, J. (2016) Seasonal cycle of precipitation over major river basins in south and Southeast Asia: a review of the CMIP5 climate models data for present climate and future climate projections. *Atmospheric Research*, 180, 42–63. https://doi.org/10.1016/j.atmosres.2016.05.008.

UN. (2015). About the Sustainable Development Goals—United Natins Sustainable Development. *Sustainable Development Goals*.

Verdon, D.C. and Franks, S.W. (2006) Long-term behaviour of ENSO: interactions with the PDO over the past 400years inferred from paleoclimate records. *Geophysical Research Letters*, 33(6), L06712. https://doi.org/10.1029/2005GL025052.

Veres, M.C. and Hu, Q. (2013) AMO-forced regional processes affecting summertime precipitation variations in the Central United States. *Journal of Climate*, 26, 276–290. https://doi.org/10.1175/JCLI-D-11-00670.1.

Villafuerte, M.Q. and Matsumoto, J. (2015) Significant influences of global mean temperature and ENSO on extreme rainfall in Southeast Asia. *Journal of Climate*, 28, 1905–1919. https://doi.org/10.1175/JCLI-D-14-00531.1.

Walsh, K.J.E., Mcbride, J.L., Klotzbach, P.J., Balachandran, S., Camargo, S.J., Holland, G., Knutson, T.R., Kossin, J.P., cheung, L.T., Sobel, A. and Sugi, M. (2016) Tropical cyclones and climate change. *Wiley Interdisciplinary Reviews: Climate Change*, 7, 65–89. https://doi.org/10.1002/wcc.371.

Wang, B. and Fan, Z. (1999) Choice of south Asian summer monsoon indices. *Bulletin of the American Meteorological Society*, 80, 629–638. https://doi.org/10.1175/1520-0477(1999)080<0629:COSASM>2.0.CO;2.

Wang, B., Wu, R. and Lau, K.M. (2001) Interannual variability of the asian summer monsoon: contrasts between the Indian and the Western North Pacific-east Asian monsoons. *Journal of Climate*, 14, 4073–4090. https://doi.org/10.1175/1520-0442(2001)014<4073:IVOTAS>2.0.CO;2.

Wang, B., Wu, Z., Li, J., Liu, J., Chang, C.P., Ding, Y. and Wu, G. (2008) How to measure the strenght of the east Asian summer monsoon. *Journal of Climate*, 21, 4449–4463. https://doi.org/10.1175/2008JCLI2183.1.

Wang, C.-C., Lee, W.-L. and Chou, C. (2019) Climate effects of anthropogenic aerosol forcing on tropical precipitation and circulations. *Journal of Climate*, 32(16), 5275–5287.

Wang, W., Lu, H., Yang, D., Sothea, K., Jiao, Y., Gao, B., Peng, X. and Pang, Z. (2016) Modelling hydrologic processes in the Mekong River basin using a distributed model driven by satellite precipitation and rain gauge observations. *PLoS One*, 11, e0152229. https://doi.org/10.1371/journal.pone.0152229.

Westra, S., Alexander, L.V. and Zwiers, F.W. (2013) Global increasing trends in annual maximum daily precipitation. *Journal of Climate*, 26, 3904–3918. https://doi.org/10.1175/JCLI-D-12-00502.1.

Wibig, J., Jaczewski, A., Brzóska, B., Konca-Kędzierska, K. and Pianko-Kluczyńska, K. (2014) How does the areal averaging influence the extremes? The context of gridded observation data sets. *Meteorologische Zeitschrift*, 23, 181–187. https://doi.org/10.1127/0941-2948/2014/0470.

World Bank. (2013). Turn down the Heat: Climate Extremes, Regional Impacts, and the Case for Resilience. The World Bank.

Xie, S.P., Deser, C., Vecchi, G.A., Ma, J., Teng, H. and Wittenberg, A.T. (2010) Global warming pattern formation: sea surface temperature and rainfall. *Journal of Climate*, 23, 966–986. https://doi.org/10.1175/2009JCLI3329.1.

Xue, Z., Liu, J.P. and Ge, Q. (2011) Changes in hydrology and sediment delivery of the Mekong River in the last 50 years: connection to damming, monsoon, and ENSO. *Earth Surface Processes and Landforms*, 36(3), 296–308. https://doi.org/10.1002/esp.2036.

Yang, R., Zhang, W.K., Gui, S., Tao, Y. and Cao, J. (2019) Rainy season precipitation variation in the Mekong River basin and its relationship to the Indian and East Asian summer monsoons. *Climate Dynamics*, 52, 5691–5708. https://doi.org/10.1007/s00382-018-4471-1.

Yao, J. and Chen, Y. (2015) Trend analysis of temperature and precipitation in the Syr Darya Basin in Central Asia. *Theoretical and Applied Climatology*, 120, 521–531. https://doi.org/10.1007/s00704-014-1187-y.

Yatagai, A., Arakawa, O., Kamiguchi, K. and Kawamoto, H. (2009) A 44-year daily gridded precipitation dataset for Asia. *Solaiat*, 5, 137–140. https://doi.org/10.2151/sola.2009.

Yatagai, A., Kamiguchi, K., Arakawa, O., Hamada, A., Yasutomi, N. and Kitoh, A. (2012) APHRODITE: constructing a long-term daily gridded precipitation dataset for Asia based on a dense network of rain gauges. *Bulletin of the American Meteorological Society*, 93(9), 1401–1415. https://doi.org/10.1175/BAMS-D-11-00122.1.

Yin, J., Yin, Z., Zhong, H., Xu, S., Hu, X., Wang, J. and Wu, J. (2011) Monitoring urban expansion and land use/land cover changes of Shanghai metropolitan area during the transitional economy (1979-2009) in China. *Environmental Monitoring and Assessment*, 177, 609–621. https://doi.org/10.1007/s10661-010-1660-8.

Yue, S., Pilon, P., Phinney, B. and Cavadias, G. (2002) The influence of autocorrelation on the ability to detect trend in hydrological series. *Hydrological Processes*, 16, 1807–1829. https://doi.org/10.1002/hyp.1095.

Zahn, R. (2009) Beyond the CO_2 connection. *Nature*, 460, 335–336. https://doi.org/10.1038/460335a.

Zhang, C., Tang, Q. and Chen, D. (2017b) Recent changes in the moisture source of precipitation over the tibetan plateau. *Journal of Climate*, 30, 1821–1837. https://doi.org/10.1175/JCLI-D-16-0493.1.

Zhang, L., Wu, P. and Zhou, T. (2017a) Aerosol forcing of extreme summer drought over North China. *Environmental Research Letters*, 12(3), 034020. https://doi.org/10.1088/1748-9326/aa5fb3.

Zhang, R.H. and Levitus, S. (1997) Structure and cycle of decadal variability of upper-ocean temperature in the North Pacific. *Journal of Climate*, 10, 710–727. https://doi.org/10.1175/1520-0442(1997)010<0710:SACODV>2.0.CO;2.

Zhang, W. and Zhou, T. (2019) Significant increases in extreme precipitation and the associations with global warming over the global land monsoon regions. *Journal of Climate*, 32(24), 8465–8488. https://doi.org/10.1175/JCLI-D-18-0662.1.

Zhang, X., Alexander, L., Hegerl, G.C., Jones, P., Tank, A.K., Peterson, T.C., Trewin, B. and Zwiers, F.W. (2011) Indices for monitoring changes in extremes based on daily temperature and precipitation data. *Wiley Interdisciplinary Reviews: Climate Change*, 2, 851–870.

Zhao, A.S., Stevenson, D.S. and Bollasina, M.A. (2019) The role of anthropogenic aerosols in future precipitation extremes over the Asian Monsoon Region. *Climate Dynamics*, 52, 6257–6278. https://doi.org/10.1007/s00382-018-4514-7.

Zhu, Y., Sang, Y.-F., Chen, D., Bellie, S. and Li, D. (2020) Effects of the Indian summer monsoon anomaly on seasonal variations of precipitation over the South-Central Tibetan Plateau. *Environmental Research Letters*, 15, 124067.

Ziv, G., Baran, E., Nam, S., Rodriguez-Iturbe, I. and Levin, S.A. (2012) Trading-off fish biodiversity, food security, and hydropower in the Mekong River Basin. *Proceedings of the National Academy of Sciences*, 109(15), 5609–5614. https://doi.org/10.1073/pnas.1201423109.

Zolina, O., Simmer, C., Belyaev, K., Gulev, S.K. and Koltermann, P. (2013) Changes in the duration of European wet and dry spells during the last 60 years. *Journal of Climate*, 26, 2022–2047. https://doi.org/10.1175/JCLI-D-11-00498.1.

Zolina, O., Simmer, C., Belyaev, K., Kapala, A. and Gulev, S. (2009) Improving estimates of heavy and extreme precipitation using daily records from European rain gauges. *Journal of Hydrometeorology*, 10, 701–716. https://doi.org/10.1175/2008JHM1055.1.

Zolina, O., Simmer, C., Gulev, S.K. and Kollet, S. (2010) Changing structure of European precipitation: longer wet periods leading to more abundant rainfalls. *Geophysical Research Letters*, 37(6), L06704. https://doi.org/10.1029/2010GL042468.

SUPPORTING INFORMATION

Additional supporting information may be found in the online version of the article at the publisher's website.

How to cite this article: Irannezhad, M., Liu, J., & Chen, D. (2021). Extreme precipitation variability across the Lancang-Mekong River Basin during 1952–2015 in relation to teleconnections and summer monsoons. *International Journal of Climatology*, 1–25. https://doi.org/10.1002/joc.7370